RSC Advances

REVIEW

View Article Online
View Journal | View Issue

Cite this: *RSC Adv.*, 2025, **15**, 16766

A review on perovskite oxides and their composites as electrode materials for supercapacitors

Mugil Neelakandan,†[ae] Preethi Dhandapani,†[b] Senthilkumar Ramasamy,[c] Ramesh Duraisamy,*[d] Seung Jun Lee*[e] and Subramania Angaiah*[ae]

In energy storage applications, supercapacitors serve as an alternative to electrochemical batteries due to their large power density and exceptionally long cycle life. Redox-active supercapacitors are favoured for their durability and power density arising from the carbon-dominated field. However, their commercialization is questioned due to their slow reaction kinetics and low energy density limitations. Electrode materials with superior electrochemical behaviour must be developed to overcome these obstacles. The oxygen anion-intercalation mechanism leads to an interest in perovskite oxide materials with intrinsic oxygen vacancies and flexible structural characteristics. The primary objective of this review is to present an overview of the fundamental characteristics of perovskite oxides, their charge storage mechanism, and the key factors governing the electrochemical behaviour of the active material. This review was also compiled by reviewing previous research on perovskite materials for supercapacitors. This study examines the anion-intercalation mechanism and the variables affecting the electrochemical performance of electrodes. Furthermore, this review addresses the challenges and significance of previous research. Moreover, it presents the design guidelines for perovskite materials for supercapacitors, which appear beneficial for future studies on these materials.

Received 19th March 2025
Accepted 24th April 2025

DOI: 10.1039/d5ra01950h

rsc.li/rsc-advances

1. Introduction

In the field of energy conversion and storage, supercapacitors (SC), Li-ion batteries, and fuel cells are gaining more attention. To close the gap between conventional capacitors and rechargeable batteries, SCs are viewed as a new kind of energy storage device because of their high-power density, ultrafast charge–discharge rate, low internal resistance, long cycling life, and wide operating temperature (from −40 to 70 °C).[1–5] SCs generally operate through two distinct mechanisms: Electric Double-Layer Capacitance (EDLC) and pseudo capacitance. The fundamental mechanism in EDLCs is electrostatic adsorption, which results in the formation of charges at the electrode–electrolyte interface.[6,7] Conversely, pseudocapacitors have charge storage through the faradaic reaction between electroactive species, which helps in achieving better charge density. The charge storage capacity of pseudocapacitors, which relies on redox reactions, surpasses that of EDLC by 10–100 times.[8,9] This significant enhancement is attributed to the rapid faradaic process employed in pseudocapacitance for charge storage, as opposed to the electrostatic adsorption mechanism in EDLC.[10,11] Although Transition Metal Oxides (TMOs), including MnO_2 and Co_3O_4, are considered cost-effective and promising electrodes for SC, their widespread adoption in SC applications is significantly hindered by their poor energy density and limited cycling lifespan.[12–14] During redox reactions in perovskite oxides (PO) within the electrolyte, the oxygen vacancies associated with the oxygen ion intercalation mechanism explain the oxygen ion insertion and extraction process.[15] As oxygen vacancies carry charges, it is well known that controlling their concentration is one of the most efficient and simplest paths for increasing the capacitance of the materials used for oxygen ion intercalation.[16] A-Site and B-site doping techniques in ABO_3 have been demonstrated to modify intrinsic physicochemical properties, including electrical conductivity, catalytic activity, ferromagnetism, and oxygen vacancies.[17] Moreover, constructing lattice distortion can produce abundant oxygen vacancies. On the other hand, oxygen ion's insertion and extraction capabilities are influenced by the variable valence of B-site ions which is observed in the lattice of perovskite-type oxides.[18] As a result, hetero ion doping can alter the perovskite's lattice structure and improve its electrochemical characteristics.[19] The primary PO for supercapacitors includes single perovskite oxide

[a]*Electro-Materials Research Laboratory, Centre for Nanoscience and Technology, Pondicherry University, Pondicherry-605 014, India. E-mail: subramania@gmail.com*
[b]*Department of Physics, National Central University, Taoyuan 32054, Taiwan*
[c]*Center of Excellence in Advanced Materials and Green Technologies, Amrita School of Engineering, Amrita Vishwa Vidyapeetham University, Coimbatore-641112, India*
[d]*Dept of Chemistry, College of Natural & Computational Sciences, Arba Minch University, P.O. Box 21, Arba Minch, Ethiopia. E-mail: ramesh.duraisamy@amu.edu.et*
[e]*Dept of IT-Energy Convergence (BK21 FOUR), Korea National University of Transportation, Chungju-27469, Republic of Korea. E-mail: sjlee@ut.ac.kr*
† The authors are equally contributed.

(ABO_3), double perovskite oxide ($AA'BB'O_{6-\delta}$), triple perovskite oxide ($AA'A''BB'B''O_{9-\delta}$), Ruddlesden–Popper (RP, $A_2BO_{4-\delta}$), and other derived perovskite-type oxides.[20–22] Single perovskite oxides have been extensively studied in lanthanide-based (La-based) perovskites, including $LaMnO_3$, $LaFeO_3$, $LaCoO_3$, and $LaNiO_3$, due to their high voltage window and excellent stability. $LaNiO_3$ demonstrated the highest specific capacitance (C_{sp}) of 719 F g^{-1} in neutral electrolyte.[23,24] However, leaching cations in the aqueous electrolyte can damage the crystal structure of a single perovskite oxide.[25] The electrochemical stability of SC is enhanced by the more stable structure of double and triple perovskite oxides, which feature a mixed arrangement of distinctions.[26,27] Moreover, they exhibit wider voltage windows, which increases the energy density of SC according to the energy density calculation formula, $E = \frac{1}{2}CV^2$, where C and V represent the working electrode's specific capacitance (C_{sp}) and potential window, respectively, and also highlight the SC's application potential.[28,29] Meanwhile, the power density is calculated by the formula $P = (E \times 3600)/\Delta t$ where E and Δt represents energy density and discharge time. In particular, under various reduction conditions, the rapidly scattered lattice elements of a simple double perovskite oxide ($AA'B_2O_6$) can be transformed into an ordered structure with a uniform distribution of A-site cations. Faster oxygen kinetics are promoted by the internally ordered structure of double perovskite oxides compared to the disordered structure in solid oxide fuel cells.[30,31] For SC, the ordered structure facilitates the concentration of oxygen vacancies. Sr_2CoMoO_6 and $PrBaMn_2O_6$, two prominent double perovskite oxides, have been studied as electrode materials.[32–35] Sr_2CoMoO_6 demonstrates a B-site-ordered rock-salt structure, whereas $PrBaMn_2O_6$ exhibits an A-site-ordered structure. According to the description, the internally ordered structure can offer a more convenient electron transmission path and more oxygen vacancies than the disordered counterpart. Liu *et al.* noted an ultrahigh C_{sp} of 1571 F g^{-1} for $Pr_{0.5}Ba_{0.5}Mn_{1.7}Co_{0.3}O_{6-\delta}$ with Co_3O_4 on the double perovskite surface.[36] It utilized the decay of specific transition metal ions in double perovskite oxide within an H_2 atmosphere.[37] The use of triple and double POs is expanding quickly, and more practical methods of enhancing their functionality in SC have been created.[36] Moreover, as of the rapid development, a current conclusion is necessary to systematically describe the most recent development direction in SC with a perovskite oxide electrode in recent years. It will serve as both a rapid reference and an inspiration for creative approaches for future research. This paper compiles the modification guidelines for PO, including morphological design, doping strategy, and composite formation with other materials.[33] The phase transition transformation process under a reduced environment and the modifications induced by the segregation of B-site metal ions are explicitly discussed for double perovskite oxide.

2. Types of perovskites

2.1 Single perovskite oxides

Perovskite materials have served as a substance for several decades. A perovskite structure embodies an ideal configuration characterized by an A-cubic crystal and ABO_3 stoichiometry lattice, which belongs to the space group *Pm3m* (Fig. 1). The components of this structure consist of a three-dimensional framework created by corner-sharing BO_6 octahedra. Perovskite oxide with the formula ABO_3 has a distorted structure, oxygen vacancy concentration, and high tap density, where A represents the alkaline rare earth, and B represents the transition rare earth elements.[38] Element A possesses a larger ionic radius than element B, and other metal elements can be substituted for the ions at both the A and B sites. PO doped with varying physicochemical characteristics, such as polarity, specific surface area, and electrical conductivity, enable the exploitation of this property.[38–40] As a result, PO holds enormous promise for use in solar cells, superconductors, catalysts, and sensor materials.

The oxygen atom is present at the centre of each of the 12 sides, the centre of the cube's body is A-cations, and each of the eight corners is called B-cations while examining the structure of PO. Considering the A site at the cubic corner position (0, 0, 0), the face-centred position of the oxygen atom will be located at the cubic lattice ($\frac{1}{2}$, $\frac{1}{2}$, 0), and the B cation occupies the body-centred position ($\frac{1}{2}$, $\frac{1}{2}$, $\frac{1}{2}$), while the A cation is visible with 12-coordination to the oxygen anion (Fig. 2). Therefore, the B–O bond distance is $a/2$, and the A–O bond distance is $a/\sqrt{2}$, where a is the cubic unit cell parameter.[41,42] The radii of the A-site and B-site ions must satisfy the formula $t = (r_A + r_x)/\sqrt{2}(r_B + r_x)$, which results in the formation of the required perovskite structure. The tolerance of the cubic system is $t = 1$, which represents the optimal value for the perovskite structure. Adjusting the octahedral factor μ-value ($\mu = r_B/r_x$) between 0.44 and 0.90 and the t-value between 0.89 and 1.0 aids in forming the ideal cube-shaped perovskite structure and regulates the

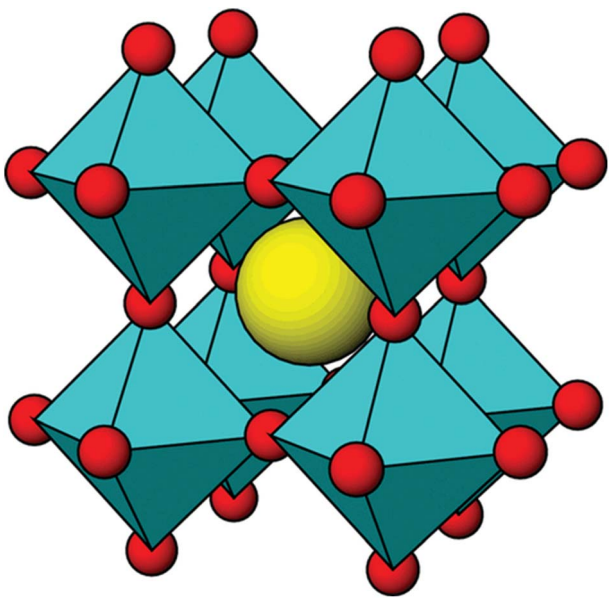

Fig. 1 Ideal cubic perovskite structure for ABO_3 (BO_6 units – cyan; A atoms – yellow; O atoms – red).[38] This figure has been reproduced from ref. 38 with permission from *Frontiers in Chemistry*, copyright 2025.

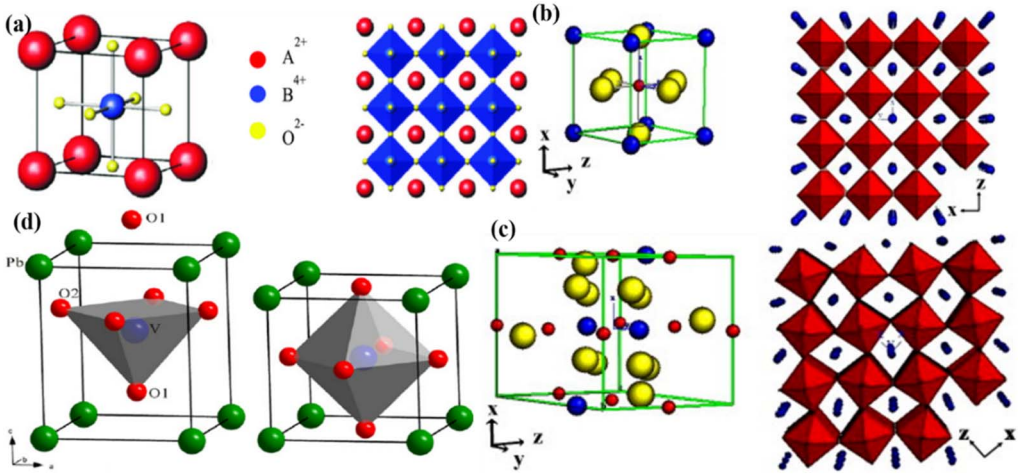

Fig. 2 Different structures of perovskite material (a) cubic, (b) monoclinic, (c) orthorhombic and (d) tetragonal.[41,42] This figure has been reproduced from ref. 41 and 42 with permission from Elseiver, copyright 2025.

stability of the octahedra. Moreover, A–O and B–O bond lengths will vary when a significant portion of the atoms in the A and B sites are changed for other elements. Therefore, a popular technique for enhancing the properties of perovskites is to dope with numerous cations of different ionic radii and valence to substitute the A and B site cations fractionally. The current value of $\mu = 0.59$ can form the BX_6 structure, which enhances the stability of the perovskite. When tilting the crystal structure of perovskite ABO_3, octahedra are formed, leading to the development of crystal phases such as triclinic, monoclinic, orthogonal, tetragonal, and rhombohedral (Fig. 2).[42–45]

2.2 Double perovskite oxides

Perovskite oxides (ABO_3) can result in the formation of double perovskite oxides when half of the B site cation is replaced by one cation.[38,42,45] Meanwhile, the cations of the A and B sites are positioned in the resulting structures, such as $A'A''BO_6$ (double A site) and $AB'B''O_6$ (double B site) (Fig. 3).[48] The expansion of a basic perovskite oxide unit results in the formation of double perovskite oxides, where the A and A′ cations are enclosed within cub-octahedrons, while the B and B′ cations occupy the central positions of octahedrons in the double perovskite oxide structure.[49,50] The appropriately ordered B′ and B″ cations are necessary for the double perovskite $A_2B'B''O_6$ crystal structure.[46,47] There are three primary types: layered B-cation sublattice structures, rock salt, and columns. Bochu *et al.* initially identified these materials, where an additional transition metal (the A′ site) occupies 75% of the A site.[51] This can lead to the emergence of two possible structures: an A site-ordered quadruple perovskite ($AA'_3B_4O_{12}$) or a 1 : 3-type A site cation arrangement ($AA'_3B_2B'_{16}O_{12}$). High-pressure techniques are generally necessary to synthesize these quadruple perovskites, ensuring the cation is accurately positioned in the A′ site under square planar conditions.[51,52] Alternatively, the B site is adaptable and can accommodate cation variability. One of the

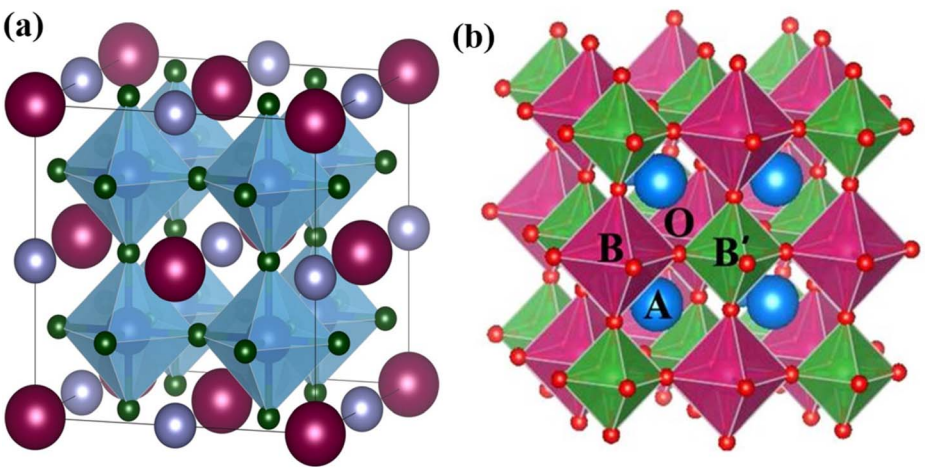

Fig. 3 Schematic illustration of (a) $A'A''BO_6$ (double A site), (b) $AB'B''O_6$ (double B site).[46,47] This figure has been reproduced from ref. 46 and 47 with permission from RSC, copyright 2025.

distinctive structural and electronic properties of these structured quadruple perovskites is A′–B intersite charge transfer. The A and B sites promote ferroelectricity, while the A′–B–B′ spin interactions are strengthened, leading to elevated spin ordering temperatures.[53–55] Kumar *et al.* investigated the electrochemical performance of R_2MMnO_6 perovskite oxides (R = La, Gd; M = Zn, Cu, Ni). The prepared electrode namely La_2ZnMnO_6, La_2CuMnO_6, and Gd_2NiMnO_6 exhibited specific capacitances of 718.6 F g^{-1}, 205.5 F g^{-1}, and 400.46 F g^{-1}, respectively, at varying current densities.[56,57] Further, to enhance supercapacitor characteristics, improving specific surface area and increasing charge transfer at the nanoscale are found to be effective measures.[58,59] Meng *et al.* synthesized a hollow spherical porous structure of La_2CoMnO_6 through template impregnation (HS-LCMO).[60] In comparison, La_2CoMnO_6 was synthesized using the sol–gel method (SG-LCMO). The specific surface area of HS-LCMO and SG-LCMO was found to be 22.14 and 10.36 m^2 g^{-1}, respectively.[60]

2.3 Triple perovskite oxides

More precise configurations, such as triple POs ($A_3BB'_2O_9$) and the perovskite family, offer a straightforward method for exploring structure–property relationships due to their ability to adopt various distinct stacking sequences. They can also accommodate a variety of metal cations, including those with unpaired electrons, in unique crystallographic positions with flexible bond angles.[49] Their general formula is typically $A_3B'B''_2O_9$ or $A_3B_3O_9$, where the specific arrangement of cations is crucial in determining the material's overall properties. The A-site cations (*e.g.*, La, Sr, Ba, Ca) typically occupy a cubic or distorted cubic lattice, providing structural stability. In contrast, two transition metal (B-site) cations occupy distinct positions within the octahedral network. The crystal structure is significant for basic and applied research in any chemical system, including triple perovskites.[43] The triple perovskite oxide can be divided into hexagonal and non-hexagonal systems depending on the material's structural distortion. Most systems belong to hexagons, while others belong to non-hexagonal crystal structures like monoclinic and orthorhombic. The hexagonal triple perovskite may contain a 6H hexagonal structure with unique 3-fold or 6-fold rotational symmetry, which undergoes crystallization belonging to $P6_3/mmc$ and $P6_3mc$ space groups, respectively. These crystal systems are named 6H–A and 6H–B triple perovskite system.[61] Fig. 4 shows the schematic representation of (a) 6H–A and (b) 6H–B crystal systems. In non-hexagonal triple perovskite systems, the 6H–A crystal structure transforms to other structures like monoclinic or orthorhombic due to structural distortion, as shown in Fig. 4c. This primarily depends on the amplitude of distortion caused by the cationic size mismatches in the system and accompanied by the modulation of face-sharing octahedra-polymers.[61,62]

The specific capacitance of PO has been significantly enhanced through the various modification techniques, leading to an expansion in the energy density of these materials. Among the key innovations is extending the voltage window, which directly contributes to improving the energy density of SC. The unique crystal structure of PO allows for incorporating different metal components, making them highly suitable for improving the voltage range in SC. A notable example is the triple perovskite oxide $Sr_3CoFeMoO_{9-\delta}$, proposed by Qiao, demonstrating distinct redox potentials for its metal components—Co, Fe, and Mo. The specific arrangement of these metals, influenced by the Fe elements against inductive effects, leads to a long voltage window of 1.4 V for $Sr_3CoFeMoO_{9-\delta}$ (SCFM). Furthermore, the voltage profile from the GDC curve demonstrated exceptional stability at different current densities, indicating consistent performance under varying conditions. The material exhibited excellent capacitance retention, with 74.6% of the C_{sp} preserved at a scanning speed of 10 mV s^{-1}. These characteristics highlight the potential of PO, particularly SCFM, as advanced materials for next-generation supercapacitors with enhanced stability and energy density. The symmetrical supercapacitor SCFM‖SCFM exhibited a power density of 1412.9 W kg^{-1} and an energy density of 58.5 W h kg^{-1} within a potential window of 1.4 V.[63] The supercapacitors fabricated with this electrode material demonstrated an C_{sp} of 685 F g^{-1} at a 2.0 A g^{-1} current density. The partial substitution of Mn^+ at the B-site was pivotal in

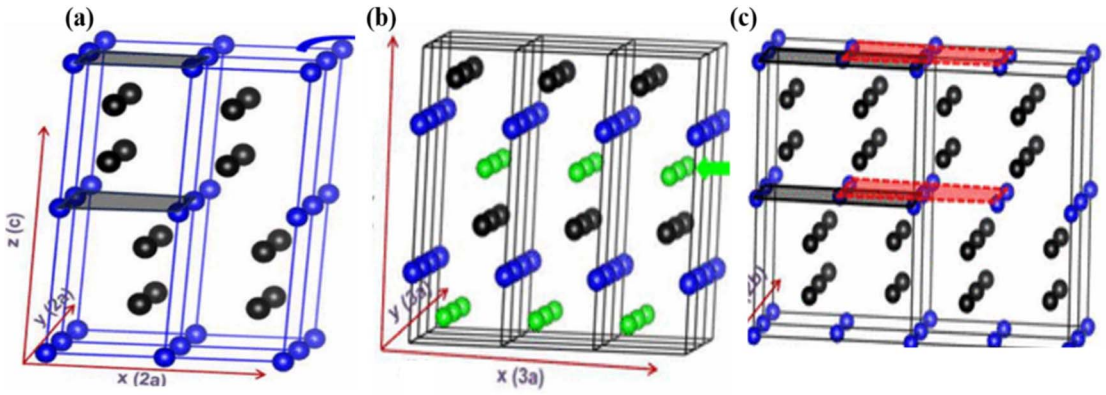

Fig. 4 Schematic representation of (a) 6H-A and (b) 6H–B and (c) orthorhombic crystal systems.[61,62] This figure has been reproduced from ref. 61 and 62 with permission from RSC, copyright 2025.

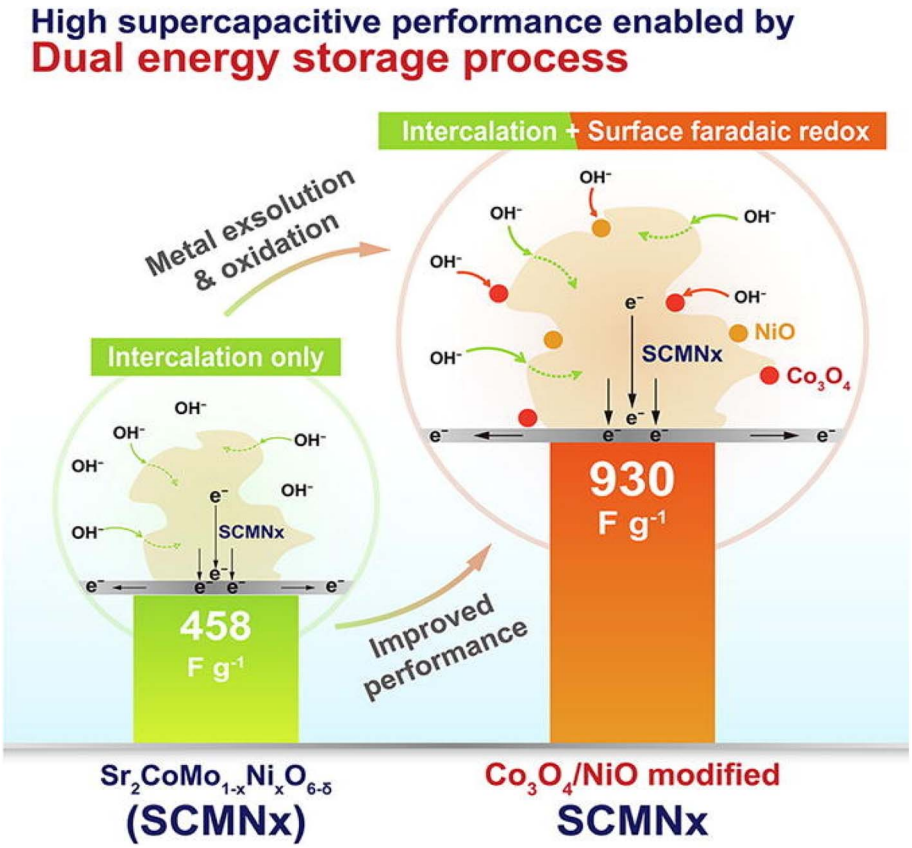

Fig. 5 Charge storage mechanism of $Sr_2CoMo_{1-x}Ni_xO_{6-\delta}$.[65] This figure has been reproduced from ref. 65 with permission from Elseiver, copyright 2025.

enhancing the oxidation state of Fe cations and promoting the mobility of oxygen ions through oxygen vacancy sites. Moreover, the electrochemical stability of LBFM-0.2 was rigorously evaluated by subjecting it to extended charge–discharge cycles, showcasing its potential for practical applications. After 3000 charge–discharge cycles, the supercapacitor retained approximately 94% of its initial capacity.[64] Yin Qiao synthesized $SrFe_{1-x}Zr_xO_{3-\delta}$ by using a solid-state synthesis method. Zr substitution enhances the structural stability in comparison with the pure $SrFeO_{3-\delta}$. The fabricated electrode demonstrates a suitable C_{sp} of 163.92 F g^{-1} and excellent cycling stability.[63] Liu *et al.* synthesized $Sr_2CoMo_{1-x}Ni_xO_{6-\delta}$ using the sol–gel method. The prepared electrode enables two distinct forms of energy storage, including faradaic surface redox pseudocapacitance and oxygen anion-intercalation pseudocapacitance, as shown in Fig. 5. The electrode exhibits enhanced electrochemical performance, demonstrating a C_{sp} of 930 F g^{-1}.[65] Furthermore, Zhu *et al.* synthesized $SrCo_{0.9}Nb_{0.1}O_{3-\delta}$ (SCN) using the ball milling method, which exhibits stability at 95.7% of its original capacity after 3000 cycles with a high energy density of 37.6 W h kg^{-1}.[64,66] Hence, double perovskite oxide clarifies its well-ordered structure and specific surface modification engineering, whereas triple perovskite oxide offers the advantages of a diverse metal element arrangement.

3. Charge storage mechanism in perovskite oxides

Due to their simple cost, large skeletal structure, high charge density, and basic properties like oxygen vacancies and chemical tunability, PO have attracted much interest.[67,68] These materials have been widely used as useful substances in energy-related applications for several years. Meffold efforts towards the study of the oxygen anion intercalation process in nanostructured lanthanum-based PO was an important historical moment.[69] The method follows like this: first, oxygen diffuses as OH^- ions from the electrolyte. Within the crystal lattice, these OH^- ions increase in the edges of the octahedral structures and fill the oxygen vacancies. Water is produced due to the oxidation of two Mn^{2+} ions to Mn^{3+} simultaneously. Intercalation of excess oxygen occurs at the material's surface in the next reaction phase. As shown in Fig. 6, this involves the oxidation of two Mn^{3+} ions to Mn^{4+} and the release of manganese to the surface.[70] As mentioned earlier, most PO are essential for charge storage. Other metal oxides that rely on positive ions such as Li^+ or Na^+ for charge transfer, including TiO_2–B, T–Nb_2O_5, and α-MoO_3, demonstrated similar intercalation behaviour. On the other hand, O^{2-} ions in PO are very useful and can store multiple times as much charge per cycle as Li^+ intercalation.[71,72] PO are also considered upcoming materials for supercapacitors

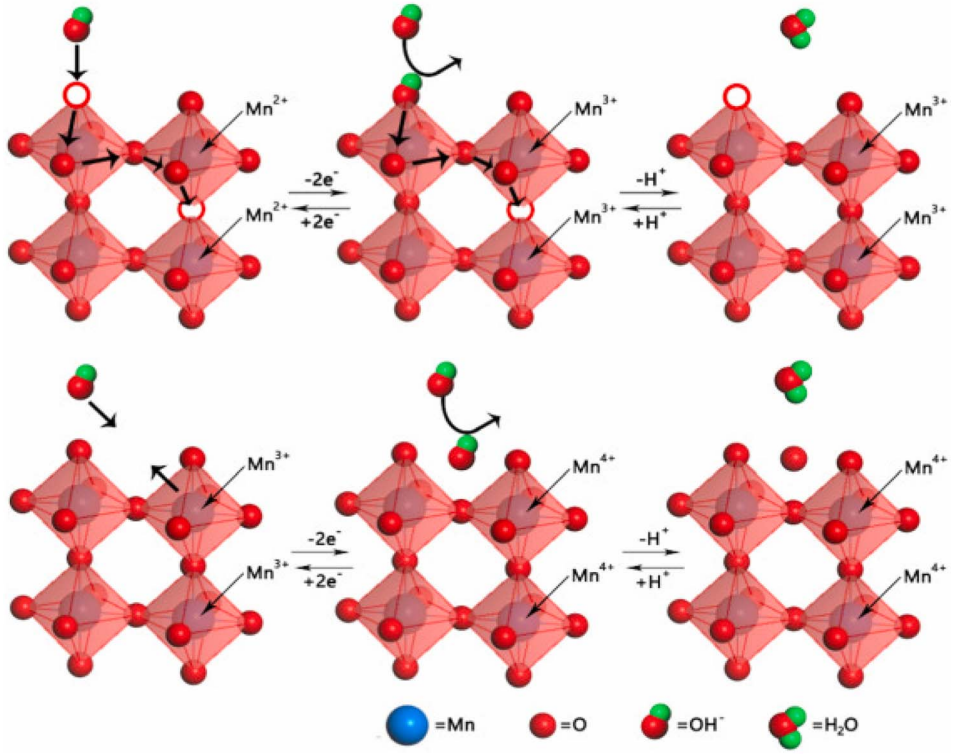

Fig. 6 Schematic illustration of oxygen intercalation mechanism in PO.[70] This figure has been reproduced from ref. 70 with permission from Elseiver, copyright 2025.

due to this characteristic. The idea is that O^{2-} ions have greater intercalation pseudocapacitance because they can carry two negative charges per unit.

4. Synthesis methods of perovskite oxides

4.1 Microwave synthesis method

There are several benefits of using vapour-phase synthesis for introducing and managing nanostructures. Electromagnetic waves with high frequency and wavelengths ranging from 1 mm to 1 m, specifically microwaves operating within the frequency range of 0.3 to 300 GHz, are utilized. They are frequently employed for both cooling and heating purposes. The microwave approach uses heating mechanisms, including ionic conduction and depolarization, which heat molecules or ions through collisions and friction. Chemical reactions are efficiently enhanced by this method.[73] Fig. 7 illustrates the schematic representation of the microwave synthesis method. Chen *et al.* used vapor-phase synthesis at high temperatures to synthesis $CsSnI_3$, which displayed a low surface combination rate and a long carrier diffusion length (~1 μm). The $CsSnX_3$ precursor powder was heated to 280 °C and then produced to a mica substrate ($[KAl_2(Si_3Al)O_{10}(OH)_2]$) by flowing argon gas to enable the controlled growth of nanowires. Bulk synthesis, melting, and colloidal processes are standard synthesis techniques for PTO.[76]

Due to perovskite's outstanding characteristics that have made it easy to modify, several manufacturing methods have been developed, with the solvothermal approach being one of the most widely used. To create Ru-based perovskite/graphene nanocomposites, Hassan *et al.* used the redox reactions that were started by heating using thermal and microwave assistance. Both techniques utilized direct redox interactions between GO and Ru precursors.[74–76] According to structural research and material characterizations, the microwave-assisted method developed more well-ordered nanoparticles, while thermal heating yielded better reduction efficiency.[77] Kostyukhin *et al.* utilized microwave heating to synthesize lanthanum orthoferrite ($LaFeO_3$) perovskites to address the issue of extended synthesis durations.[76] This microwave method accelerates $LaFeO_3$ particle growth and crystallization through surface polarization and localized overheating. This method provided a more efficient method for material creation than hydrothermal synthesis, decreasing the synthesis time by about 10 hours.[76]

4.2 Sol–gel method

The sol–gel technique allows for precise control over composite particle's uniformity and particle size. However, it typically requires multiple complex agents, extended processing times, and stringent parameters such as specific temperatures and pH.[78] Controlling the structure of oxides produced by the sol–gel technique is challenging, and the intrinsic instability of the structure restricts its application. Despite being highly homogenous and not requiring high processing temperatures, nanomaterials are frequently created in polycrystalline form.[79] Fig. 8 illustrates the schematic representation of PO using the

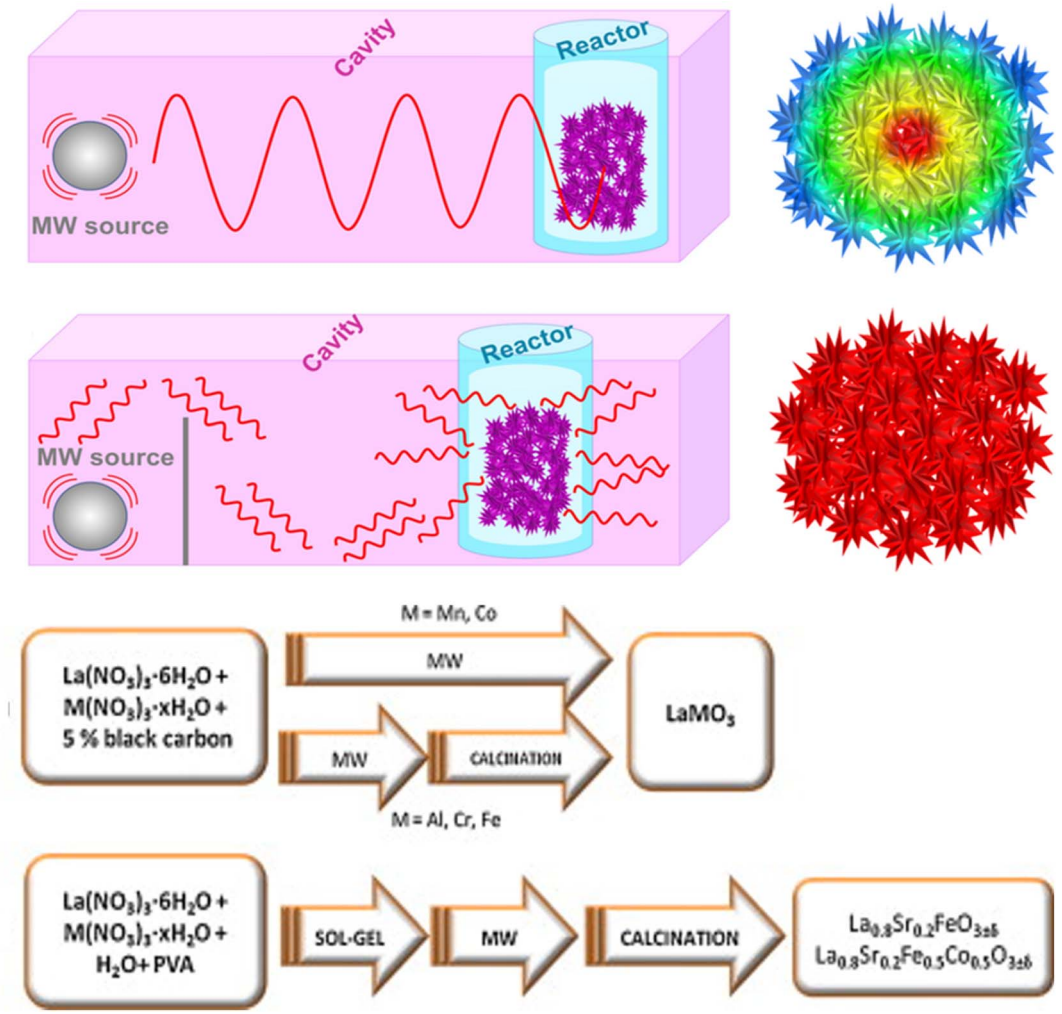

Fig. 7 Schematic representation of the microwave synthesis method.[74,75] This figure has been reproduced from ref. 74 and 75 with permission from RSC, copyright 2025.

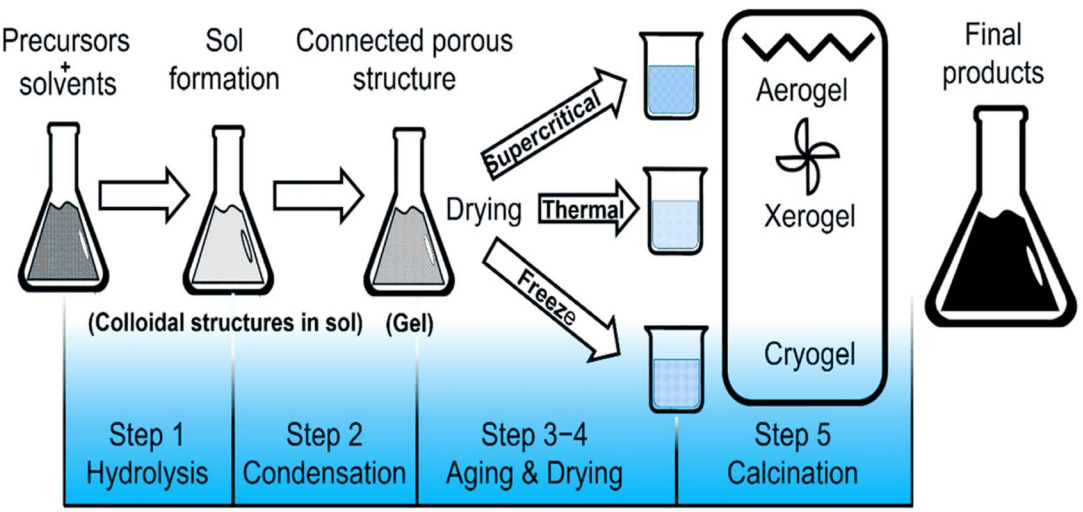

Fig. 8 Schematic representation of POs by the sol–gel method.[80] This figure has been reproduced from ref. 80 with permission from Elseiver, copyright 2025.

sol–gel method.[80] Kharangarh *et al.* used the sol–gel and hydrothermal methods in a process that involved two steps to create a high-conductivity electrode material. Initially, the $SrCo_{0.9}Mo_{0.1}O_{3-\delta}$ (SCM) perovskite had been generated by doping molybdenum into cobaltite using the sol–gel technique. Graphite was finally added to the SCM using the hydrothermal process. Due to increased oxygen vacancies, SCM showed better cycle life and specific 440 F g^{-1}.[81] Hu *et al.* synthesized $CsPbX_4$ NCs in a covalent solvent to create advanced $CsPbX_3$ NCs using a water-assisted transformation method. The surface of perovskite NCs at the hexane/water interface was then functionalized through an effective sol–gel modification approach. With this method, monodisperse $CsPbX_3/SiO_2$ and $CsPbBr_3/Ta_2O_5$ were effectively produced. At the hexane/water contact, it is notable that change and oxide attachment took place at the same time.[82] Zhang *et al.* successfully produced $LaFeO_3$ perovskite nanoparticles using a sol–gel method by utilizing the porosity properties of MOF templates and advanced methods. The new technique performed exceptionally well, offering more relaxed preparation conditions, easier preparation, and flexible processing intervals. The procedure started with systematically mixing La salt, Fe salt, and the organic ligand H_3BTC in an ethanolic solution to create the first product (MOG-La-Fe). After MOG-La-Fe was pyrolyzed on an appropriate substrate, mesoporous $LaFeO_3$ perovskite nanoparticles were produced. At a power density of 900 W kg^{-1}, these materials demonstrated outstanding energy efficiency of 34 W h kg^{-1}.[83,84] Tomar *et al.* synthesized $SrTiO_3$ perovskite oxide nanofibers. The synthesis of $SrTiO_3$ nanostructures was carried out by sol–gel method, then heating at various temperatures. Consequently, the generated electrode exhibits improved electrochemical characteristics, including increased C_{Sp}, high-rate capability 208.47 F g^{-1}, better cyclic stability at 1500 cycles and longer cycle life.[85] Tomar *et al.* synthesized $SrTiO_3$ using the sol–gel method for PO with a cubic structure. Consequently, the $SrTiO_3$ cubic structure offers several benefits, such as being environmentally friendly and having a specific surface area, enhancing supercapacitor performance with a high specific surface area and an efficient mass transfer rate of electrolyte ions. The fabricated symmetric supercapacitor exhibited a higher C_{Sp} of approximately 212.5 F g^{-1} at 0.63 A g^{-1} with improved cyclic stability and excellent capacitance retention of about 99% after 5000 continuous cycles.[85] Shereef *et al.* synthesized double perovskite La_2NiMnO_6 by the sol–gel technique. At a current density of 0.1 A g^{-1}, the material exhibited a reduced specific capacity of 9.16 F g^{-1}.[86] Jose *et al.* reported the synthesis of La_2FeMnO_6, demonstrating high specific capacitance, good electrical conductivity, and long-term cycle stability. The mesoporous capacitance of La_2FeMnO_6 reached up to 10.9 mF g^{-1}, with excellent capacitance retention of 96% after 5000 cycles.[87]

4.3 Solvothermal method

In the solvothermal technique, the solvent is nonaqueous, which is how it varies from the hydrothermal approach. On the other hand, hydrothermal synthesis produces the desired product by reacting precursors in a solution containing water, usually at high temperatures and pressure.[88] Riaz *et al.* employed a solvothermal approach to produce $KCdCl_3$/rGO and $KCdCl_3/C_{60}$. More reactive sites, efficient charge/ion movement, exceptional cycle stability, and high C_{Sp} are among the benefits provided by $KCdCl_3/C_{60}$ in electrochemical processes.[89] Hussain *et al.* synthesized hollow spherical perovskite fluoride $NaNiF_3$ using a one-step solvothermal process, as shown in Fig. 9. The asymmetric supercapacitor (SC) made with $NaNiF_3$/AC

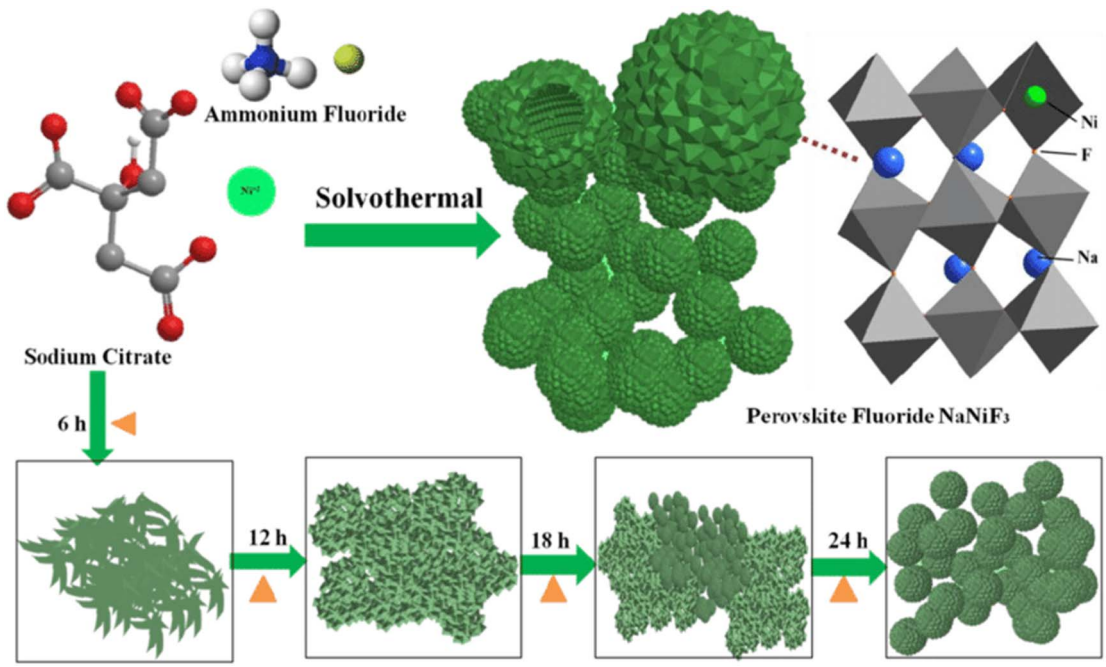

Fig. 9 Synthesis process of hollow spherical $NaNiF_3$ perovskite fluoride nanocrystals.[90] This figure has been reproduced from ref. 90 with permission from Wiley, copyright 2025.

electrodes demonstrated a high energy density of 51.78 W h kg^{-1} at 1.65 kW kg^{-1}, a wide electrochemical window (1.65 V), and excellent cycling durability, maintaining 100% capacity retention from 1400 to 10 000 cycles. The production mechanism of hollow spherical perovskite fluoride has also been investigated.[90] N. Bibi *et al.* hydrothermally produced $SrZrO_3$ nanorods with high electrical conductivity, porosity, and cyclic stability. Therefore, the as-synthesized electrode demonstrates remarkable capacitance retention over 1000 cycles and a capacitance of 1225 F g^{-1} at a current density of 10 A g^{-1}. Additionally, the fabricated electrode achieves a maximum power density of 4000 W kg^{-1} and an energy density of 65 W h kg^{-1}.[91]

4.4 SILAR method

SILAR is regarded as a relatively straightforward and economical technique for thin-film deposition, allowing for accurate control over thickness and composition.[92,93] The method entails the repetition of four-step sequential adsorption, rinsing, reaction, and rinsing stages, leading to the layer-by-layer growth of thin films (Fig. 10). This layer-by-layer deposition mechanism enables precise film thickness and composition control, which can be fine-tuned by altering parameters such as precursor concentration, immersion time, and reaction conditions. In the 1980s, Nicolau *et al.* introduced the successive ionic layer adsorption and reaction (SILAR) method for fabricating thin films.[95] Subsequently, a modified pseudo-SILAR (p-SILAR) method was developed for synthesizing doped and binary/ternary nanocomposites (NCs). Yasmeen *et al.* reported the synthesis of perovskite $CsPb_2Br_5$ nanocomposites using the SILAR method. It has been demonstrated that SILAR and p-SILAR are straightforward, cost-effective, rapid, and scalable synthesis techniques that involve exposing a substrate film or particles to ionic precursors, leading to (1) cation adsorption, (2) washing, (3) anion reaction, and (4) further rinsing.[96] For instance, Ghule *et al.* synthesized nano pebbles-like $BiVO_4$@C electrodes by the SILAR method. The following are the steps in the systematic method for the deposition of $BiVO_4$@C: (1) the first beaker containing the cationic precursor ($Bi(NO_3)_3$ + BGBE) was submerged in the cleaned FSSM substrate for 10 s. During this time, Bi^{3+} ions were adsorbed onto the substrate due to the force of attraction between the ions in the solution and the substrate surface. (2) To eliminate the weakly bound Bi^{3+} ions, the FSSM substrate was submerged in the second beaker filled with double-distilled water for ten seconds. (3) In order to create stable $BiVO_4$@C thin films, the previously adsorbed Bi^{3+} ions reacted with VO_4^{3-} ions in the third beaker containing the anionic precursor (NH_4VO_3 + BGBE) for 10 seconds. (4) The substrate was rinsed with DDW for ten seconds in the fourth beaker to eliminate extra or unreacted species. During 5000 GCD cycles, the $BiVO_4$@C electrodes exhibited enhanced cycling performance with 94.6% capacitive retention.[97]

4.5 Electrospinning method

Electrospinning is a complex yet cost-effective method to fabricate nanotubes and nanofibers with diameters ranging from several micrometres to tens of nanometers. Additionally, beyond the size and structure, it also depends on other factors such as the concentration of the parent compound, the viscosity of the parent compound solution, the type of polymer, and the electrospinning parameters, including voltage, working distance, and feed rate, which are other crucial factors (Fig. 11).[98] In the case of supercapacitors, the perovskite-type metal oxide is a reliable electrode material with remarkable capacitive performance. Due to the high concentration of oxygen vacancies in these perovskites, they exhibit outstanding electrochemical properties. The supercapacitor based on La_x-$Sr_{1-x}NiO_{3-d}$ ($0.3 \leq x \leq 1$) NFs demonstrated exceptional

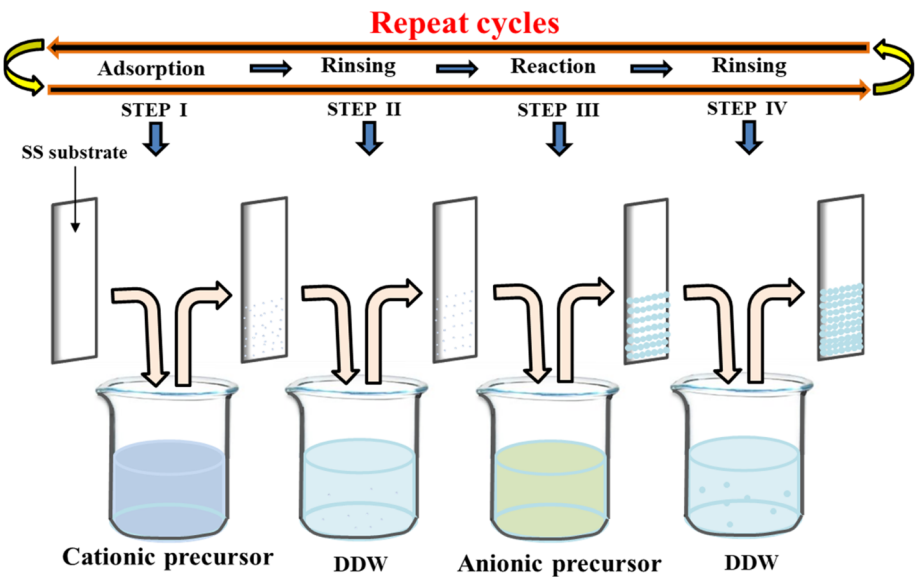

Fig. 10 Schematic representation of SILAR method.[94] This figure has been reproduced from ref. 94 with permission from Elseiver, copyright 2025.

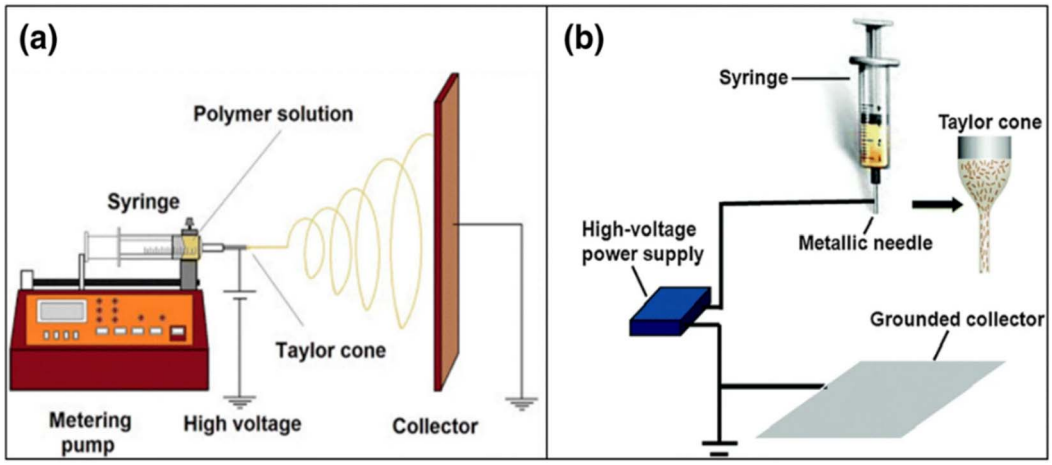

Fig. 11 Schematic diagram of set up of electrospinning apparatus (a) horizontal set up and (b) vertical setup.[98] This figure has been reproduced from ref. 98 with permission from Elseiver, copyright 2025.

electrochemical characteristics, achieving 719 F g^{-1} at 2 A g^{-1}.[99] Similarly, $La_xSr_{1-x}Co_{0.1}Mn_{0.9}O_{3-\delta}$ ($0.3 \leq x \leq 1$) NFs demonstrated a capacitance of 485 F g^{-1} at 1 A g^{-1} in 1 M KOH. Similarly, the supercapacitive performance of $SrMnO_3$ NFs has been investigated concerning the effects of doping Ba, Ca, and Ni on the Sr site and Co, Fe, and Ni on the Mn site, respectively. The study revealed that adding 20 mol% Ba to the $SrMnO_3$ matrix enhanced capacitance from 321.7 F g^{-1} to 446.8 F g^{-1} at 0.5 A g^{-1}.[100]

5. Strategies of perovskite oxides on the performance of supercapacitors

5.1 A-Site doping

Generally, the supercapacitor performance of perovskite oxides is directly linked to the B-site transition metal element. The A-site component, which consists of alkaline earth and lanthanide elements, is typically inert in the redox reaction. However, the cation at the A-site may influence the electronic coordination and structure. A significant improvement occurs when a low-valence cation partially replaces the A-site, causing some B-site transition-metal ions to shift to unstable oxidation states $(B^{m+}/B^{(m+1)})^+$ redox pair, such as Sr^{2+} and Ca^{2+}. This alteration also generates additional oxygen vacancies. Consequently, the electrochemical performance is enhanced, and electronic conductivity increases. It is environmentally advantageous for alkaline earth metals to replace rare earth metals due to their similar atomic radii. In this context, Roy *et al.* utilized a sol–gel technique to synthesize Ca-doped perovskite lanthanum manganates ($La_{0.5}Ca_{0.5}MnO_3$). The C_{Sp} of $La_{0.5}Ca_{0.5}MnO_3$ was 2.4 times higher than that of pure $LaMnO_3$.[101,102] Similarly, Wang *et al.* doped $LaMnO_3$ with Sr and observed that after 1000 cycles, the cycle life enhanced from 40% to 80%, and the capacitance slightly increased from 187 to 198 F g^{-1} at 0.5 A g^{-1}. Meanwhile, Tian *et al.* used the sol–gel method to synthesize $La_{1-x}Sr_xMnO_3$ ($x = 0$, 0.15, 0.3, 0.5) to understand better how the substitution degree influences electrochemical performance.[103] It was discovered that the value of x influences the charge transfer resistance, C_{Sp}, and degree of nanoparticle aggregation.[103] A group of PO with the composition $La_{1-x}Sr_x$-BO_{3-d} ($x = 0$–1; B = Fe, Mn, Co) was recently synthesized by Wang *et al.* to investigate anion-based pseudocapacitors systematically. They found that the surface-normalized capacity, whose slope is determined by the B-site element, increases linearly with a higher oxygen vacancy content following the systematic addition of Sr^{2+}.[102] Compared to the Fe and Co oxides, $La_{0.2}Sr_{0.8}MnO_{2.7}$ exhibited the highest C_{Sp} of approximately 492 F g^{-1}. The energy required for the aliovalent substitution of oxygen vacancies depends on the alkaline-earth metals. Luo *et al.* investigated the influence of Ba and Ca doping on $SrMnO_3$ nanofibers. By doping the $SrMnO_3$ matrix with 20 mol% Ba, the C_{Sp} significantly increased from 321.7 F g^{-1} to 446.8 F g^{-1}. Furthermore, the $Sr_{0.8}Ba_{0.2}MnO_3$ based ASC demonstrated excellent capacitance retention of 87% after 5000 cycles and an energy density of 37.3 W h kg^{-1} at a power density of 400 W kg^{-1}.[104]

5.2 B-Site doping

Cobalt-based PO exhibit greater efficiency than Mn-based ones due to their enhanced oxygen-ion mobility and higher concentration of oxygen vacancies. Certain cobalt-based PO such as cubic phase, at room temperature $SrCoO_{3-\delta}$, are unstable. Sharma *et al.* partially substituted Mo for Co in $SrCoO_{3-\delta}$ to widely deploy cobalt-based PO in SCs (Fig. 12a).[34] It was found that $SrCo_{0.9}Mo_{0.1}O_3$ (SCM) had 2.1 times more oxygen vacancies than $SrCoO_{3-\delta}$. Furthermore, compared to $SrCoO_{3-\delta}$, SCM exhibits a C_{Sp} of approximately 1223.34 F g^{-1} at 1 A g^{-1} (Fig. 12b). Notably, after 10 000 cycles, the ASC, utilizing lacey-reduced graphene oxide nanoribbon (LRGONR) as the negative electrode, demonstrated long-term stability (Fig. 12c). At a power density of 734.5 W kg^{-1}, it also achieved a specific energy density of 74.8 W h kg^{-1} (Fig. 12d).[105] Similarly, Shao *et al.* reported Nb-doped $SrCoO_{3-\delta}$ with a gravimetric capacitance of approximately 773.6 F g^{-1} and excellent cycling

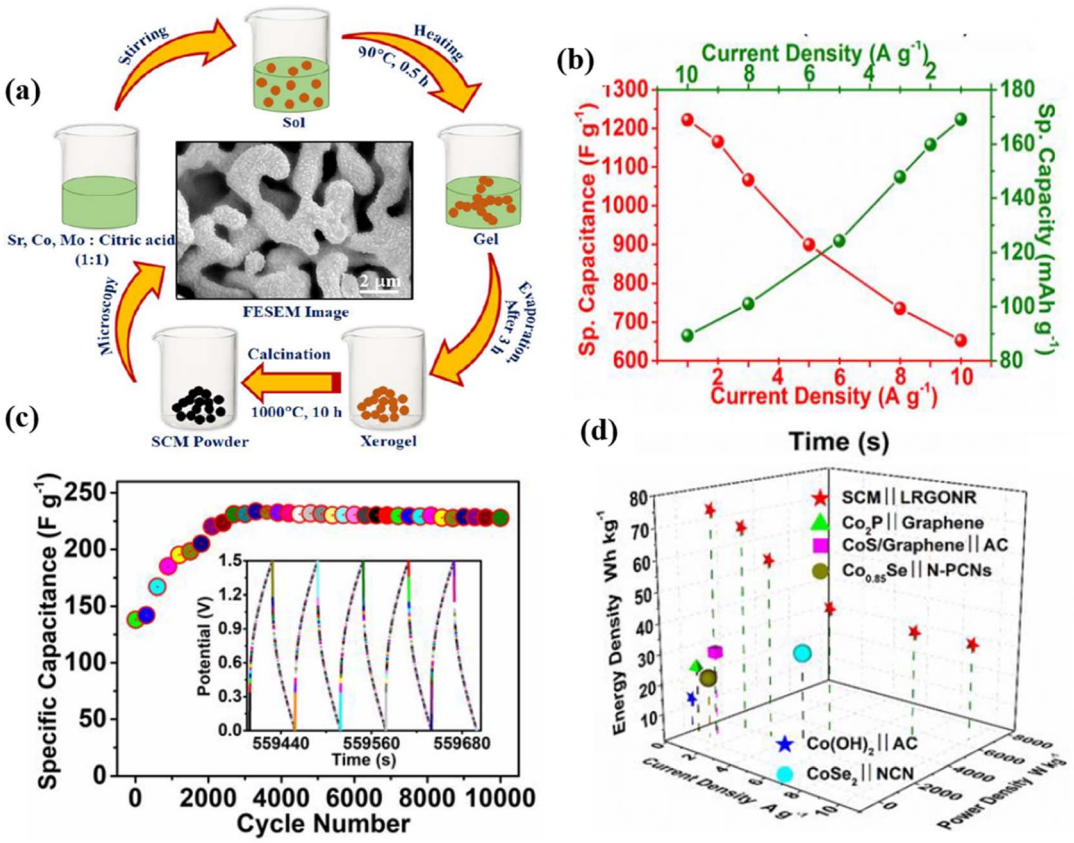

Fig. 12 (a) Schematic representation of the synthesis process of SCM. (b) GCD curves of the SCM electrode at varying current densities. (c) Cycling stability of the ASC at 10 A g^{-1}. The inset displays the final five GCD cycles. (d) Ragone plot of a hybrid SCM cell compared with literature findings.[98] This figure has been reproduced from ref. 98 with permission from Elseiver, copyright 2025.

stability, exhibiting about 95.7% capacitance retention after 3000 cycles. Additionally, an ASC was assembled with AC and $SrCo_{0.9}Nb_{0.1}O_{3-\delta}$ (SCN), serving as the cathode and anode, respectively. When the power density was 433.9 W kg^{-1}, the device's energy density reached 37.6 W h kg^{-1}, and when the power density increased to 9864.2 W kg^{-1}, it continued to maintain an energy density of 32.9 W h kg^{-1}. Furthermore, the potential window of PO may be influenced by B-site doping.[64] G. Singh *et al.*[105] explored the impact of B-site element doping on the stability window of $SrRuO_3$. Notably, it was found that doping $SrRuO_3$ with 20 mol% Mg enhanced its C_{Sp} without altering its stability window. Conversely, substituting Fe or Co could lead to a reduced stability window.

5.3 Modulating stoichiometry

Various post-processing techniques, including heat treatment at elevated temperatures in an environment with low oxygen partial pressure and inert conditions, are used in a reducing atmosphere like H_2 to produce oxygen-deficient POs with the general formula $ABO_{3-\delta}$. According to research by Mefford *et al.*, sub-stoichiometric $LaMnO_{2.91}$ performed better than anion excess form $LaMnO_{3.09}$.[106] Oxygen vacancy concentration and overall performance are also significantly impacted by cation deficiencies. The influence of cation stoichiometry in $LaMnO_3$ was explored by Qian *et al.* by manipulating the A and B-site cation ratio. The $LaMn_{1\pm x}O_{3-\delta}$ outperformed the stoichiometric $LaMnO_3$. Although supercapacitor performance was not specifically examined, perovskites with A-site cation deficiency have been demonstrated to produce oxygen-deficient structures.[107] Fig. 13 shows the synthesis process of different perovskite oxide powders.

6. Design of perovskite electrode materials

Design principles for perovskite electrode materials can be clarified based on the charge storage mechanism of the perovskite oxide electrode. These principles can be classified into the following sections.

6.1 Creating oxygen vacancy

According to the perovskite oxide structure theory, substituting the A site with a low valence can enhance the valence of the B site element or increase the oxygen vacancy concentration.[108] The oxygen vacancy concentration is only marginally influenced by replacing the A site with a high valence, which may reduce the valence of the B or A sites. As the concentration of oxygen vacancies increases, more hydroxide anions intercalate through

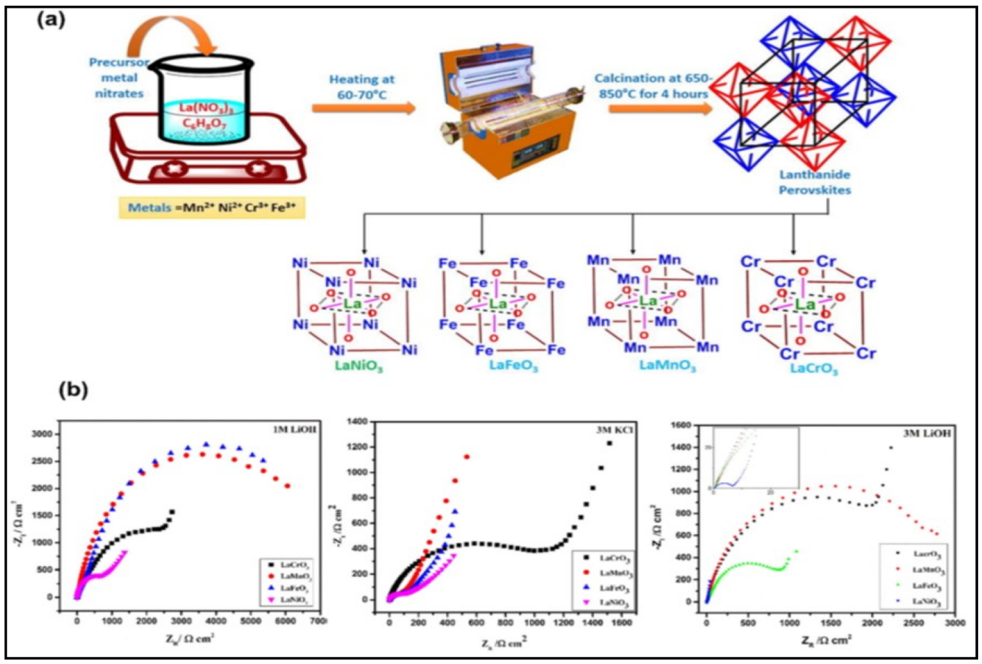

Fig. 13 (a) Synthesis procedure for four types of different perovskite oxide powders ($LaMnO_3$, $LaFeO_3$, $LaCrO_3$, and $LaNiO_3$) for application as SC anode materials using the sol–gel method. (b) EIS of the four perovskite materials in various electrolyte solutions.[107] This figure has been reproduced from ref. 107 with permission from Elseiver, copyright 2025.

the electrode surface and diffuse from the electrolyte to the electrode more efficiently.[109] However, elevating the B site element's valence restricts the theoretical C_{Sp}. Consequently, enhancing the electrochemical performance of perovskite by replacing the A site with low valence is an inefficient technique. Even though achieving theoretical specific capacitance is highly challenging, the approach can enhance electrochemical performance due to its partially diminished internal resistance and capability to facilitate diffusion and intercalation quantity.[110–112] The internal resistance of perovskite, which affects the electrode's power density, is influenced by the B–O–B bond length and angle, which are determined by the atomic size and the type of doped element. While certain perovskite structures have been identified, accurately measuring the crystal structure's B–O–B bond angle and length remains a significant challenge.[113] These bond angles and lengths require first-principles simulations for a more precise explanation. The relationship between bond angle, length, and doped element can be analyzed through perovskite material design in conjunction with first-principles simulations. Additionally, it can calculate the theoretical internal resistance of perovskite, which may help reduce the development cycle of doped perovskite design.[114]

In conclusion, C_{Sp} and power density can be optimized by developing element-doped perovskite oxides with high oxygen vacancies and minimal internal resistance. Several examples of suitable composition selection are provided, including Ti, Nb, Mo, and V, whose oxides have been used as electrodes to fabricate electrochemical capacitors. With high valence states, these elements doped in the B site can enhance the oxygen vacancy in perovskites.[115,116]

6.2 Designing the microstructure and high specific surface area

A large specific surface area can enhance the C_{Sp} and ion exchange rate between electrodes and electrolytes. The advantages of different microstructures for supercapacitors vary.[117,118] A core–shell structure can improve the electrode's cycle stability by limiting the core material's phase transition. The electrode's resistance can be reduced by shortening the electron transfer path from the active material's surface to the current collector using a nanoneedle or nanosheet structure. Perovskites with various nanostructures are expected to exhibit higher C_{Sp}, longer cycle stability, greater power density, and increased energy density.[119,120] However, there is still much to discover due to different microstructures were created through hydrothermal reactions, guiding agents like urea, hexamine, and ammonium hydroxide, which stop hydroxide coprecipitation from happening when lanthanum-based perovskites are being prepared. Although the sol–gel method can produce flower-like and nanowire perovskites, these structures are unsuitable for *in situ* growth on the surface of the current collector.[121,122] Therefore, to achieve successive coprecipitation or obtain perovskite *in situ*, further research should focus on developing a novel guiding agent for the hydrothermal reaction of perovskite. Binder-free *in situ* growth can improve the electrochemical performance of perovskites by preventing issues related to poor conductivity.[123,124]

First, at the perovskite calcination temperature, conventional current collectors such as carbon paper and nickel foam undergo significant oxidation in the air. Therefore, protection with argon or nitrogen is necessary. Second, the formation of

perovskite is impeded by certain transition metal hydroxides, like $Mn(OH)_2$, $Ni(OH)_2$, and $Co(OH)_2$, which can only be converted into diatomic metal oxides and cannot undergo further oxidation when protected by nitrogen or argon.[125] Consequently, it is essential to prepare the trihydroxide before calcination. As a result, Fe and Ti, which can exist as $Fe(OH)_3$ and $Ti(OH)_3$, are promising candidates for *in situ* perovskite production. In conclusion, hydrothermal reactions are necessary to produce perovskites with a wider range of microstructures, but careful selection of guiding agents and B-site components is essential to obtain the desired perovskites.[126]

6.3 Developing perovskite composites

Three main components comprise the design concept for perovskite composites: initially, perovskites can be combined with oxides whose potential window partially overlaps the perovskite's potential window. Furthermore, this kind of perovskite composite can enhance its integral potential window.[127,128] At the same time, the energy density of composites is enhanced when the specific capacitance is either minimally affected or even increased by the extended potential window. Additionally, perovskites can be combined with oxides with a different redox potential than the perovskites themselves. This enables simultaneous charge storage at competing active sites during the charging process, enhancing the specific capacitance. The combination of $La_{0.85}Sr_{0.15}MnO_3$ with $NiCo_2O_4$ was recently explored, addressing the challenge of binder-free electrodes for perovskites with a core–shell architecture. This material demonstrated remarkable electrochemical performance, including a high specific capacity of 260.75 mA h g^{-1} at 0.5 A g^{-1} in 6 M KOH. Additionally, it demonstrated exceptional cycle stability, retaining 200% after 10 000 cycles at a current density of 20 A g^{-1}. When incorporated into hybrid supercapacitors, it achieved an energy density of 63.5 W h kg^{-1} at a power density of 900 W kg^{-1}.[129] The high electrochemical performance can be attributed to the synergistic interaction of Mn, Co, and Ni, coupled with the excellent contact between the active materials and the current collector. Lastly, perovskites can be combined with a conductor to form a composite. Even though perovskites have good electrical conductivity, most cannot match conductor conductivity. Combining perovskites with conductors can further enhance electrochemical performance due to resistance affecting power density and SpC.[130]

7. Applications of perovskite oxides towards supercapacitors

Previous studies suggest that the defective structure of perovskite oxide and its enhanced oxygen ion mobility can facilitate the conversion of B^{x+} to a high valence state, thereby improving electrochemical properties. However, limitations of PO, such as their restricted surface area and high transport resistance of aggregated nanoparticles, impede further enhancement of electrochemical performance.[131,132] Combining ABO_3 with other materials, such as metal oxides, carbon materials, and noble metals, to form composites with enriched chemistry effectively solves these challenges.

7.1 Perovskite oxide based electrode materials

7.1.1 Strontium-based perovskite oxides. Strontium-based perovskite oxides have attracted considerable research attention as supercapacitor electrode materials due to their natural abundance, excellent ionic and electronic conductivity, and resistance to redox cycling. Table 1 compares the specific capacitance of various strontium-based PO. $SrFeO_3$, $SrCoO_3$, and $SrCoFeO_3$, representing three distinct perovskites, were synthesized using the sol–gel method, achieving a high density of oxygen vacancies and exceptional capacitance. Co-doping with a 1 : 1 ratio (Co/Fe) at the B site of $SrFeO_3$ decreased the C_{Sp} when applied to supercapacitors. The synthesized electrode demonstrated a C_{Sp} of approximately 60.912 F g^{-1} at a scan rate of 10 mV s^{-1}. Additionally, nitrogen adsorption and desorption measurements were conducted to gain a detailed understanding of the porosity characteristics of the synthesized samples. SEM images revealed a rough and highly porous structure that enhances the electrode's active surface area, consistent with theoretical values.[136] George *et al.* synthesized $SrMnO_3$ perovskite oxide nanofibers using a sol–gel electrospinning method followed by calcination at various temperatures.[100] The resulting electrode exhibited enhanced electrochemical properties, including a higher specific capacitance, excellent rate capability (446.8 F g^{-1} at 0.5 A g^{-1}), improved cyclic stability (87% at 5000 cycles), and extended cycle life. The device fabricated with these nanofibers demonstrated a specific energy of 37.3 W h kg^{-1} at a specific power of 400 W kg^{-1}, proving its effectiveness as an electrode material for high-rate charge–discharge performance in supercapacitors. Lei *et al.* synthesized $SrCoTiO_3$ using a solid-state reaction method. However, it exhibited the major drawback of poor electrochemical activity as an electrode material with C_{Sp} of 114.4 F g^{-1}.[133] Using the solid-state reaction method, Lei *et al.* synthesized $SrBNbO_3$ (where B = Mn, Co). The subsequent electrochemical performance of an asymmetric supercapacitor demonstrated a higher C_{Sp} of about 894 F g^{-1} at 1 A g^{-1} with a capacitance retention of 88.88% after 10 000 cycles.[133]

7.1.2 Lanthanum-based perovskite oxides. Lanthanum-based perovskite oxides have gained significant attention in supercapacitors due to their high thermal stability, ease of synthesis, oxygen storage capacity, low cost, and excellent electrical conductivity. $LaMnO_3$ is the first lanthanum-based

Table 1 Comparison of specific capacitance of various strontium based perovskite oxides

Electrode material	Synthesis method	Specific capacitance (F g^{-1}/mF cm^{-1})	Ref.
$Sr_2CoMoO_{6-\delta}$	Sol–gel method	747	105
$SrCo_{0.875}Nb_{0.125}O_3$	Solid state reaction	894	133
$SrCo_{0.9}Nb_{0.1}O_{3-\delta}$	Solid state reaction	774	133
Ni–$SrTiO_3$	Ball milling method	142	134
Sr_2CoSbO_6	Solid-state method	228	135

perovskite oxide to be employed in SCs. The lattice, which is deficient in cations and the presence of manganese in two oxidation states (Mn^{3+}/Mn^{4+}), leads to a stable and consistent oxygen excess in $LaMnO_3$.[137] Table 2 compares the specific capacitance of various lanthanum-based perovskite oxides. Augustyn *et al.* reported a specific capacitance of 609.8 F g^{-1} for $LaMnO_3$.[171] $LaNiO_3$ exhibits a charge storage mechanism similar to that of $LaMnO_3$ but demonstrates lower electrical resistivity (approximately 10^{-4} Ohm). Shao *et al.* employed a template-free solvothermal method to synthesize a hollow spherical structure of $LaNiO_3$, leading to a high specific capacitance (422 F g^{-1} at 1 A g^{-1}) and excellent cycle stability (83.3% capacitance retention after 5000 cycles).[172] Compared with $LaNiO_3$, $LaFeO_3$ is more stable because Fe^{3+} has a stable electronic configuration $3d^5$. Zhang *et al.* used mesoporous $LaFeO_3$ nanoparticles as an electrode material for SCs (Fig. 14a). The fabricated symmetric SC cell (SSC) exhibits a high energy density of 34 W h kg^{-1} and a power density of 900 W kg^{-1}, retaining 92.2% capacitance after 5000 cycles (Fig. 14b and c).[138] Harikrishnan *et al.* used coprecipitation to create $LaCoO_3$ nanoparticles. $LaCoO_3$ has good electrochemical redox properties due to its multiple oxidation states (+2, +3 and +4), with a C_{Sp} of 299.64 F g^{-1} at 10 A g^{-1}.[164] Hussain *et al.* synthesized a hierarchical mesoporous nanostructure of $LaCrO_3$ *via* the sol–gel method. The electrode exhibits a high C_{Sp} of 1268 F g^{-1}.[156]

7.1.3 Cerium-based perovskite oxides. Cerium-based POs are promising because of their high dielectric constant, low cost, high bandgap, and variable valence states (Ce^{3+} and Ce^{4+}).[170] For instance, Nsar *et al.* employed electrospinning followed by calcination processes to synthesize $CeMnO_3$ nanofibers (NFs).[173] It is widely accepted that A-site cations of PO do not contribute to the electronic structure near the Fermi level. However, due to cerium's high redox capability between Ce^{3+} and Ce^{4+}, the faradaic redox reaction (Ce^{4+}/Ce^{3+} and Mn^{3+}/Mn^{4+}) occurred on the $CeMnO_3$ electrode surface. $CeMnO_3$ nanofibers exhibits C_{Sp} of 159.59 F g^{-1} at 1 A g^{-1} current density. Cerium-

Table 2 Comparison of specific capacitance for various lanthanum-based perovskite oxides

Electrode material	Synthesis method	Specific capacitance (F g^{-1}/mA h g^{-1})	Electrolyte	Ref.
$LaFeO_3$	Sol–gel	241	1 M Na_2SO_4	138
La_2NiFeO_6	Solvothermal	768	2 M KOH	139
$La_{0.2}Sr_{0.8}MnO_{2.7}$	Co-precipitation	492	1 M KOH	140
$LaMnO_3$	Co-precipitation	520	0.5 M Na_2SO_4	141
$La_{0.8}Na_{0.2}Fe_{0.8}Mn_{0.2}O_3$	Modified Pechini	56	1 M H_2SO_4	141
$La_{0.8}Sr_{0.1}5MnO_3@NiCo_2O_4$	Hydrothermal	1341	6 M KOH	142
$LaMnO_3/Mn_3O_4$	One pot	135	1 M Na_2SO_4	143
$La_{1-x}Sr_xMnO_3$	Sol–gel	102	1 M KOH	144
$La_xSr_{1-x}NiO_{3-\delta}$	Electrospinning	719	1 M Na_2SO_4	145
$LaNi_{1-x}Fe_xO_{3-\delta}$	Modified Pechini	894	1 M KOH	146
$LaNiO_3$	Electrospinning	116	6 M KOH	147
La_2ZnMnO_6	Hydrothermal	718	2 M KOH	148
La_2CuMnO_6	Hydrothermal	205	2 M KOH	149
La_2FeCoO_6	Sol–gel	831	2 M KOH	150
La_2CoMnO_6	Impregnation	376	1 M Na_2SO_4	151
$La_{0.5}Ca_{0.5}MnO_3$	Sol–gel	170	1 M KOH	152
$LaNiO_3$	Solvothermal	422	6 M KOH	153
$La_{0.7}Sr_{0.3}FeO_3$	Electrospinning	523	1 M Na_2SO_4	154
La_2CoNiO_6	Solvothermal	635	2 M KOH	155
$LaCrO_3$	Sol–gel	1268	1 M LiCl	156
$LaFe_{0.5}Cr_{0.5}O_3$	Sol–gel	16	6 M KOH	157
$La_{0.85}Sr_{0.15}Mn_{0.9}Ni_{0.1}O_3$	Electrospinning	113	1 M KOH	158
$La_{0.7}Sr_{0.3}Co_{0.1}Mn_{0.9}O_{3-\delta}$	Electrospinning	485	1 M KOH	159
$Ag/La_{0.7}Sr_{0.3}CoO_{3-\delta}$	Ball milling	517	1 M KOH	160
$LaNiO_3$	Sol–gel	139	6 M KOH	161
$La_{0.7}Sr_{0.3}MnO_3$	Ball milling	393	1 M Na_2SO_4	162
$La_{1-X}Ag_XMnO_{\pm\delta}$	Co-precipitation	152	6 M KOH	163
$LaMnO_3@NiCo_2O_4$	Hydrothermal	811	6 M KOH	159
$LaCoO_3$	Co-precipitation	299	3 M KOH	164
$La_{0.8}Nd_{0.2}Fe_{0.8}Mn_{0.2}O_3$	Hydrothermal	158	3 M KOH	165
$LaCoO_3$	Plasma etching	706	6 M KOH	165
$La_{0.7}Sr_{0.3}CoO_{3-\delta}@MnO_2$	Electrospinning	570	6 M KOH	165
$LaSr_{0.85}Mn_{0.15}O_3$	Sol–gel	198	1 M KOH	166
La_2CoNiO_6	Electrospinning	335	6 M KOH	167
$La_{0.6}Sr_{0.4}NiO_{3-\delta}$	Sol–gel	115	6 M KOH	168
$La_2NiO_{4+\delta}$	Citrate method	657	3 M KOH	169
$La_{1-X}K_XFeO_{3-\delta}S$	Ceramic synthesis	662	2 M KOH	170
$LaFeO_3$	Electrospinning	183	6 M KOH	169
$LaCoO_3$	Electrospinning	95	6 M KOH	169

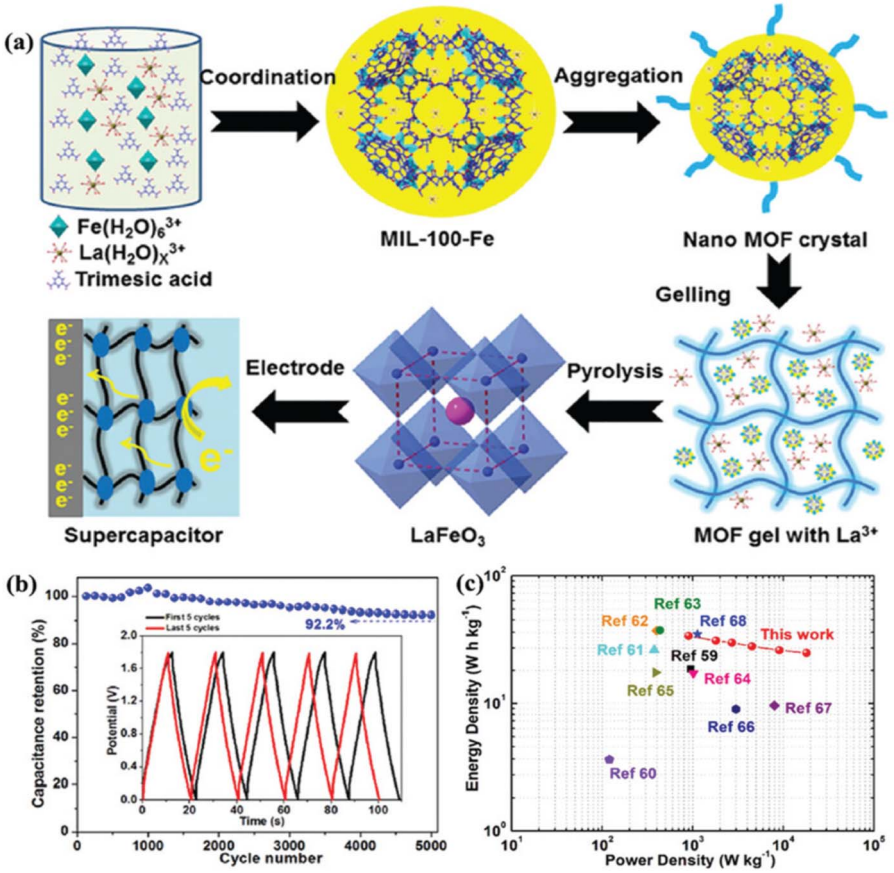

Fig. 14 (a) Schematic representations illustrating the synthesis of perovskite $LaFeO_3$. (b) Graph showing cycling stability *versus* cycle number, inset: the first and last five GCD cycles. (c) Ragone plots (energy density *vs.* power density) of this study and other devices at 2 A g^{-1}.[138] This figure has been reproduced from ref. 138 with permission from RSC, copyright 2025.

based POs ($CeCoO_3$, $CeNiO_3$, and $CeCuO_3$) have recently shown C_{Sp} of 128, 189, and 117 F g^{-1}, respectively.[174] Ahangari *et al.* compared the electrochemical properties of $CeMO_3$(M = CO, Ni, Cu), among which $CeNiO_3$ nanoplates shows high C_{Sp} of 189 F g^{-1} with good cyclic stability.[175] Harikrishnan *et al.* synthesized by coprecipitation method, and a symmetric supercapacitor was fabricated with the prepared material showing energy and power density 27 W h kg^{-1} and 826 W kg^{-1} with better cyclic stability of 92% at 5000 cycles.[176]

7.1.4 Calcium-based perovskite oxides. $CaTiO_3$, a perovskite oxide material, is attracting interest for future applications in supercapacitors. However, pure $CaTiO_3$ is not commonly used directly as an electrode material in supercapacitors due to its comparatively low electrical conductivity. Researchers focused on doping or mixing its electrochemical performance with other substances to enhance its electrochemical performance.[177,178] Lang *et al.* investigated $CaTiO_3$ combined with Activated Carbon (AC) to enhance the specific surface area and electrochemical performance of supercapacitors. The $CaTiO_3$-AC composite showed a C_{Sp} of 270 F g^{-1}, significantly higher than pure $CaTiO_3$. The activated carbon contributed to a higher surface area and better ion adsorption, improving the energy storage capacity. The composite also exhibited good long-term cycling stability.[179,180]

7.2 Perovskite oxides based composite electrode materials

7.2.1 Perovskite oxides with noble metals. The movement of electrons produced by the oxidation or reduction of PCs to the current collectors can be facilitated by noble metals, such as platinum (Pt) and gold (Au), which have good electric conductivity.[181] However, because noble metals are expensive and scarce, combining them with other affordable and sustainable materials is one of the most appealing ways to reduce their use.[182,183] One advantage of PO is that they are naturally occurring and reasonably priced. Unfortunately, PO still lack sufficient electrical conductivity. Consequently, the synergistic effects of combining PO and noble metals are anticipated to enhance their SC performance. Ag is the noble metal with the highest conductivity.[184] Moreover, it offers the benefit of an acceptable activity and a reasonable cost. Cao *et al.* synthesized an Ag nanoparticle decorated $La_{0.85}Sr_{0.15}MnO_3$ and employed it as an electrode for SC. It can create electron transfer channels because silver has a far higher electrical conductivity than carbon. The redox reaction between Ag and Ag_2O in an alkaline electrolyte solution may also slightly influence pseudocapacitance. The Ag@LSM15 composite thus produced a long cycle life retaining 100% capacitance retention after 1000 cycles and a high C_{Sp} of 186 F g^{-1} at 1 A g^{-1}.[185,186] Another study used a porous perovskite $La_{0.7}Sr_{0.3}CoO_{3-\delta}$ (LSC) substrate (Ag/LSC) to

grow Ag nanoparticles directly. The performance was examined with varying mass loadings of Ag of about 10.61, 30.60, and 51.31 mg. When the Ag content was 30 mg (30 Ag/LSC) or less, the surface became rough, and the porous structure of LSC was maintained. This advantageous structure may make more active surface sites and quicker mass transport possible. In addition, the Ag/LSC electrode with 30 mg Ag loading showed the best performance of 14.8 F cm^{-2} due to lower R_s of 1.28 Ω cm^2 and R_{ct} of 0.61 Ω cm^2.[179]

7.2.2 Perovskite oxides with metal oxides. Due to their numerous oxidation states, metal oxides have drawn increasing attention because they can store energy up to an order of magnitude more generously than carbon-based EDLCs. However, during charge/discharge processes, most metal oxides have poor durability, low conductivity, and poor rate capability. On the other hand, the stable structure of PO allows for improved surface oxygen exchange kinetics and significantly higher oxygen ion/electron conductivity.[185] Since being inexpensive and having the potential to achieve high C_{sp}/capacity values, exhibiting exceptional stability, perovskite oxide and metal oxide composites are attractive alternatives. Among the metal oxides, MnO_2 is unique because of its natural abundance, low cost, and high theoretical C_{sp} of roughly 1370 F g^{-1}. As an electrode for SCs, Jingbo *et al.* used a hydrothermal method to create a $((La_{0.75}Sr_{0.25})_{0.95}MnO_{3-\delta}(LSM)/MnO_2)$ composite. The resulting electrode exhibits a higher C_{sp} of about 437.2 F g^{-1} at 2 mV s^{-1}.[186] Although CeO_2 has distinct chemical characteristics, it has a lower theoretical capacitance than MnO_2. It is, therefore, readily oxidized and reduced throughout the oxidation-reduction process. $LaMnO_3$ mixed CeO_2 (CeO_2/$LaMnO_3$) nanocomposites with a greater C_{sp} of about 262 F g^{-1} at 1 A g^{-1} in 1 M Na_2SO_4 solution were reported by Nagamuthu *et al.* The CeO_2/$LaMnO_3$ nanocomposite worked better with ASC-negative electrodes. In particular, an ASC device was constructed with AC as the positive electrode and CeO_2/$LaMnO_3$ nanocomposites as the negative electrode. This resulted in an energy density of 17.2 W h kg^{-1} at a power density of 1015 W kg^{-1}.[187,188] The relationship between the potential window (V) and energy density (E) is well known. Therefore, expanding the potential window is an additional method of raising the energy density. Stoller *et al.* synthesized $La_{0.8}Sr_{0.15}MnO_3$@$NiCo_2O_4$ (LSM15@NC) core–shell nanoflower structure grown directly on Ni foam. LSM15@NC displayed a broad window and the coexistence of PC and EDLC behaviour. Moreover, the ASC produced an energy density of 63.5 W h kg^{-1} at a power density of 900 W kg^{-1} when the AC was used as the negative electrode and the LSM15@NC composite as the positive electrode.[189]

7.2.3 Perovskite oxides with carbonaceous materials. Carbonaceous materials with a large specific surface area, good electronic conductivity, and high chemical stability, such as graphene, reduced graphene oxide, graphene, and AC, have been used extensively in SC. The low intrinsic conductivity of perovskite oxide limits their usage in SC. An efficient method to address this shortcoming is, incorporating carbonaceous materials to create PO/carbon composites. To improve SC performance, graphene is typically added to perovskite oxides because of its superior electrical conductivity of 6000 S cm^{-1} and extra-large theoretical specific surface area of 2630 m^2 g^{-1}.[186] Agglomeration of perovskite oxides can be effectively inhibited by graphene. It can offer a fast channel for the transport of electrons in the meantime. The loading of perovskite oxide nanoparticles increases the distance between graphene sheets; they can also preserve the structural integrity of monolayer graphene. Immobilized $BiFeO_3$ (BFO) nanowires on nanometer-thin RGO show superior charge transfer resistance and C_{sp} of about 368.28 F g^{-1} compared to BFO and RGO. The electrolyte also significantly affects BFO-RGO performance, which is noteworthy.[190] To examine the capacitive behaviour of graphene–perovskite oxide compound materials in aqueous electrolytes with varying basicity or acidity, Jingbo *et al.*[186] tested reduced graphene performance sheets decorated $SrRuO_3$ (SRGO) in three different electrolytes: 1.0 M KOH, 1.0 M $NaNO_3$, and 1.0 M H_3PO_4. The SRGO showed the highest capacitance of 160 F g^{-1} in 1.0 M KOH. Adding carbon improves the electrochemical performance compared to pure PO. Pseudocapacitance is caused by the redox reaction of oxygenated groups on the surface of carbon nanostructures. Accordingly, adding heteroatoms or surface functional groups to the surface of carbon-based materials is a useful method of raising the capacitance of the composite electrode. Cheng *et al.* introduced a heteroatom to reduce graphene oxide (rGO) by substituting the hydroxyl groups with the nitrogen atoms. A three-dimensional network (LMO/N-rGO) can then be created by directly integrating the as-prepared nitrogen-doped graphene (N-rGO) sheets with $LaMnO_3$ (LMO) *via* electrostatic interactions. The resulting nanocomposites showed the best stability of 79% capacitance retention after 2000 cycles at 10 A g^{-1} and a C_{sp} of 687 F g^{-1} at 5 mV s^{-1} compared to pristine graphene and LMO.[191] In a different study, Shafi *et al.* used *in situ* chemical polymerization to create a composite material comprising $LaMnO_3$, RGO, and polyaniline (PANI). Due to the excellent structural stability and electrical conductivity offered by the RGO support and PANI coating, the synthesized ternary composite demonstrated a C_{sp} of 802 F g^{-1} at 1 A g^{-1}.[192]

7.2.4 Perovskite oxides with conducting polymers. Riaz *et al.* reported the synthesis of $KCuCl_3$-polyaniline (PANI) composites. $KCuCl_3$-polyaniline (PANI) composites have excellent electrochemical properties, with C_{sp} values as high as 1757 F g^{-1}. This high-performance is due to the positive relationship of $KCuCl_3$ conductivity and structural integrity with PANI's pseudocapacitive activity. These composites are good options for advanced supercapacitor applications due to their enhanced mechanical durability, cyclic stability, and energy storage efficiency.[193] According to the study, this improved performance was achieved by the conducting polymer's effective result with $CaTiO_3$'s strong dielectric properties, which improved cycle stability and charge storage. At a current density of 6.86 A g^{-1}, the composite showed a C_{sp} of 984.21 F g^{-1}. The power density was 3.2 kW kg^{-1}, and the energy density was 58.14 W h kg^{-1}.[194] $LaNiO_3$ nanosheets and polyazulene are promising materials for supercapacitors due to their electrochemical properties. $LaNiO_3$, a perovskite oxide, exhibits high capacitance and fast charge/discharge cycles when synthesized into nanosheet form, as shown in Fig. 15. The nanosheet morphology increases surface

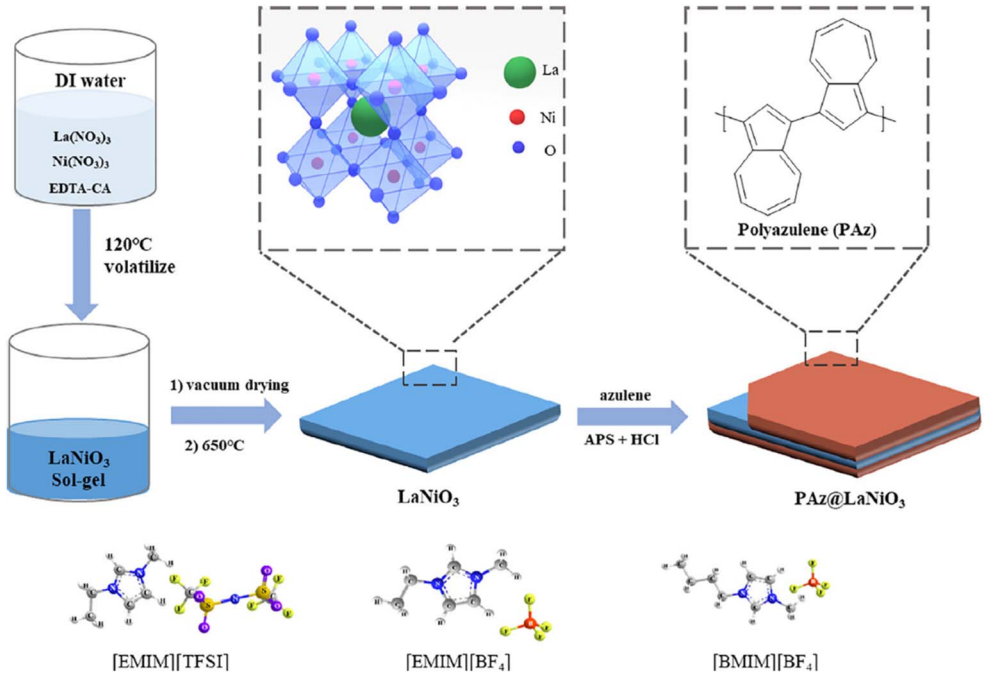

Fig. 15 Schematic representation of the preparation of PAz@$LaNiO_3$ nanosheets.[195]

area, improving electrochemical performance. Polyazulene, an organic conductive polymer, offers good conductivity and redox activity, enhancing charge storage. It undergoes reversible electrochemical reactions, making it suitable for supercapacitors. Combining $LaNiO_3$ nanoparticle nanosheets with polyazulene in composite electrodes exhibits improved capacitance and cycling stability. It exhibited a C_{Sp} of 464 F g^{-1} at a current density of 2 A g^{-1}. Thus, the material serves as a promising candidate for advanced energy storage devices.[195]

This figure has been reproduced from ref. 195 with permission from Wiley, copyright 2025.

8. Conclusion and future outlooks

Perovskite oxides (POs) have recently gained widespread attention as electrode materials for supercapacitors (SCs) due to their unique structure, compositional flexibility, and inherent oxygen vacancy. Notably, PO, as an active component in intercalation-type capacitors, possess high concentrations of oxygen vacancies and do not require significant surface area for energy storage. This article primarily compiles the recent advancements in PO (*i.e.*, single, double, and RP perovskite oxides) for SC applications. It also delves into the formation of composites and the increase in oxygen vacancy concentration to improve the electrochemical properties of PO. Despite the progress, several aspects still need to be addressed when designing future perovskite oxide electrode materials.

(1) Hydrothermal and solvothermal reactions are the primary techniques for synthesizing perovskite materials; however, their high energy requirements and costly reactants restrict large-scale synthesis. Perovskite materials with high purity and good uniformity can be synthesized using the most common synthesis techniques, such as sol–gel and solid-state methods, which use minimal energy. Therefore, it is essential to continue developing highly effective, environmentally friendly, and energy-efficient synthesis techniques.

(2) Perovskite materials are primarily determined by their oxygen vacancies, which can be created by doping, non-stoichiometric substitution, and other processes. Oxygen vacancies cause holes and redox pairs to form, which improves conductivity by promoting charge transfer. Moreover, more oxygen vacancies may promote pseudocapacitive qualities. Both A-site and B-site doping are practical methods for creating oxygen vacancies in perovskites, although B-site doping has been thoroughly and successfully investigated. In addition, excessive doping causes the crystal surface to segregate, and proper doping promotes the stability of the crystal lattice. Molecular and ionic doping can also enhance the electrochemical characteristics of perovskites. Future research must examine how co-doping A and B sites can create anionic vacancies as charge storage locations and achieve pseudo-capacitance in SCs.

(3) The morphology of the perovskite itself significantly influences the electrochemical properties of the composite. High charge mobility and quick electron transfer are made possible by the controlled scale, increased surface area, porous structure, and ion channels of nanostructures (flowers, nanoarrays, and nanorods). Carbon nanotubes (CNTs) and Activated Carbon (AC) with a large surface area were coupled with chalcocite materials to use perovskite as an electrode material for SCs with high energy and power densities and stability. The polymerization of polyazulene (PAz) on the surface of perovskite nanosheets enhances electron transfer by acting as a linker. This combination of organic and inorganic components shows both pseudo-capacitance and double-layer capacitance.

(4) The 3D bulk perovskite exhibits higher electronic conductivity than its 2D and 1D counterparts, primarily due to stronger electron-ion coupling and better orbital overlap. However, in terms of chemical and structural stability especially under environmental stressors like moisture or heat. The lower-dimensional 2D and 1D perovskites are generally more robust, owing to their layered or confined structures and often more hydrophobic organic components. Low-dimensional hybridized perovskites show promise as materials for charge storage while combining 2D and 3D materials preserves the former's stability and the latter's high efficiency.

(5) The electrochemical characteristics of the electrode material are also affected by the acidity or alkalinity of the electrolyte solution. In recent studies, perovskite bodies adsorb OH^- ions in the solution, releasing H^+ ions and oxidizing them to O_2, which, in turn, oxidizes other ions. Consequently, the alkaline electrolyte solution promotes the formation of oxygen vacancies and redox reactions. This process contributes to the high electrical conductivity observed in these materials.

(6) The electronic conductivity of RP perovskite oxides is expected to improve as their n value increases. However, most reports focus on RP perovskite oxides with $n = 1$. Consequently, RP perovskite oxides with higher n values are anticipated to be utilized as advanced SC electrode materials. Therefore, further efforts are needed to overcome the challenges presented by current research and to exploit novel perovskite materials for more promising applications.

Abbreviations

SC	Supercapacitor
PO	Perovskite oxides
C_{Sp}	Specific capacitance

Data availability

No new data were collected for this review.

Author contributions

Mugil Neelakandan – writing – original draft. Preethi Dhandapani – writing – original draft. Senthilkumar Ramasamy – reviewing & editing. Seung Jun Lee & Ramesh Duraisamy – funding acquisition, resources, reviewing & editing. Subramania Angaiah – writing – review & editing, validation, supervision, resources, funding acquisition, conceptualization.

Conflicts of interest

The authors declare no conflict of interest.

Acknowledgements

The authors gratefully acknowledge the financial support provided by the National Research Foundation of Korea (NRF) for Grant No. RS-2023-00213746 and RS-2024-00446898 under the Brain Pool Program.

References

1 A. K. Tomar, A. Joshi, G. Singh and R. K. Sharma, Perovskite Oxides as Supercapacitive Electrode: Properties, Design and Recent Advances, *Coord. Chem. Rev.*, 2021, **431**, 213680, DOI: 10.1016/j.ccr.2020.213680.

2 B. Huang, B. Xu, Y. Li, W. Zhou, Y. You, S. Zhong, C.-A. Wang and J. B. Goodenough, Li-Ion Conduction and Stability of Perovskite Li $_{3/8}$ Sr $_{7/16}$ Hf $_{1/4}$ Ta $_{3/4}$ O $_3$, *ACS Appl. Mater. Interfaces*, 2016, **8**(23), 14552–14557, DOI: 10.1021/acsami.6b03070.

3 M. Li, W. Zhou and Z. Zhu, Recent Development on Perovskite-type Cathode Materials Based on SrCoO $_{3-\delta}$ Parent Oxide for Intermediate-temperature Solid Oxide Fuel Cells, *Asia-Pac. J. Chem. Eng.*, 2016, **11**(3), 370–381, DOI: 10.1002/apj.2009.

4 B. K. Kim, S. Sy, A. Yu and J. Zhang, Electrochemical Supercapacitors for Energy Storage and Conversion, in *Handbook of Clean Energy Systems*, Wiley, 2015, pp. 1–25, DOI: 10.1002/9781118991978.hces112.

5 G. Wee, O. Larsson, M. Srinivasan, M. Berggren, X. Crispin and S. Mhaisalkar, Effect of the Ionic Conductivity on the Performance of Polyelectrolyte-Based Supercapacitors, *Adv. Funct. Mater.*, 2010, **20**(24), 4344–4350, DOI: 10.1002/adfm.201001096.

6 S. Wang, N. Liu, J. Su, L. Li, F. Long, Z. Zou, X. Jiang and Y. Gao, Highly Stretchable and Self-Healable Supercapacitor with Reduced Graphene Oxide Based Fiber Springs, *ACS Nano*, 2017, **11**(2), 2066–2074, DOI: 10.1021/acsnano.6b08262.

7 S. Yang, Y. Liu, Y. Hao, X. Yang, W. A. Goddard, X. L. Zhang and B. Cao, Oxygen-Vacancy Abundant Ultrafine Co $_3$ O $_4$/Graphene Composites for High-Rate Supercapacitor Electrodes, *Adv. Sci.*, 2018, **5**(4), 1700659, DOI: 10.1002/advs.201700659.

8 L. L. Zhang and X. S. Zhao, ChemInform Abstract: Carbon-Based Materials as Supercapacitor Electrodes, *Chem. Inf.*, 2009, **40**(47), DOI: 10.1002/chin.200947213.

9 H. Jiang, P. S. Lee and C. Li, 3D Carbon Based Nanostructures for Advanced Supercapacitors, *Energy Environ. Sci.*, 2013, **6**(1), 41–53, DOI: 10.1039/C2EE23284G.

10 R. Tummala, R. K. Guduru and P. S. Mohanty, Nanostructured Co3O4 Electrodes for Supercapacitor Applications from Plasma Spray Technique, *J. Power Sources*, 2012, **209**, 44–51, DOI: 10.1016/j.jpowsour.2012.02.071.

11 M. B. Sassin, A. N. Hoffmaster, A. M. Österholm, C. K. Lo, J. S. Ko, J. R. Reynolds and J. W. Long, Integrating Solution-Processable Conducting Polymers in Carbon Fiber Paper: Scalable 3D Electrodes for Redox-Based Supercapacitors, *ACS Appl. Polym. Mater.*, 2020, **2**(8), 3234–3242, DOI: 10.1021/acsapm.0c00382.

12 Y. Selvaraj, K. Paramasivam, M. C. Franklin, K. Sivalingam Nallathambi, V. Elayappan and H. Kuzhandaivel, Invasion of Zinc in BiFeO $_3$/Bi $_{25}$ FeO $_{40}$ Perovskite-Structured Material as an Efficient Electrode for Symmetric

Supercapacitor, *J. Phys. Chem. C*, 2024, **128**(13), 5418–5428, DOI: 10.1021/acs.jpcc.3c06729.

13 K. Iwasaki, T. Ito, M. Yoshino, T. Matsui, T. Nagasaki and Y. Arita, Power factor of La_{1-x} Sr $_x$ FeO_3 and $LaFe_{1-y}$ Ni $_y$ O_3, *J. Alloys Compd.*, 2007, **430**, 297.

14 G. A. Snook, P. Kao and A. S. Best, Conducting-Polymer-Based Supercapacitor Devices and Electrodes, *J. Power Sources*, 2011, **196**(1), 1–12, DOI: 10.1016/j.jpowsour.2010.06.084.

15 M. Rafique, S. Hajra, M. Z. Iqbal, G. Nabi, S. S. A. Gillani and M. Bilal Tahir, Fabrication of Novel Perovskite Oxide Ba $_x$ Mn $_{1-x}$ O $_3$ Electrode for Supercapacitors, *Int. J. Energy Res.*, 2021, **45**(3), 4145–4154, DOI: 10.1002/er.6075.

16 R. B. Rakhi, W. Chen, M. N. Hedhili, D. Cha and H. N. Alshareef, Enhanced Rate Performance of Mesoporous Co $_3$ O $_4$ Nanosheet Supercapacitor Electrodes by Hydrous RuO $_2$ Nanoparticle Decoration, *ACS Appl. Mater. Interfaces*, 2014, **6**(6), 4196–4206, DOI: 10.1021/am405849n.

17 J. Xu, L. Gao, J. Cao, W. Wang and Z. Chen, Preparation and Electrochemical Capacitance of Cobalt Oxide (Co3O4) Nanotubes as Supercapacitor Material, *Electrochim. Acta*, 2010, **56**(2), 732–736, DOI: 10.1016/j.electacta.2010.09.092.

18 Y. Gogotsi and R. M. Penner, Energy Storage in Nanomaterials – Capacitive, Pseudocapacitive, or Battery-Like?, *ACS Nano*, 2018, **12**(3), 2081–2083, DOI: 10.1021/acsnano.8b01914.

19 Z. Xie, H. Zhao, Z. Du, T. Chen, N. Chen, X. Liu and S. J. Skinner, Effects of Co Doping on the Electrochemical Performance of Double Perovskite Oxide Sr $_2$ MgMoO $_{6-\delta}$ as an Anode Material for Solid Oxide Fuel Cells, *J. Phys. Chem. C*, 2012, **116**(17), 9734–9743, DOI: 10.1021/jp212505c.

20 Y. Ning, Y. Pu, C. Wu, Z. Chen, X. Zhang, L. Zhang and B. Wang, Design Strategy of High-Entropy Perovskite Energy-Storage Ceramics: A Review, *J. Eur. Ceram. Soc.*, 2024, **44**(8), 4831–4843, DOI: 10.1016/j.jeurceramsoc.2024.02.040.

21 R. A. Afre and D. Pugliese, Perovskite Solar Cells: A Review of the Latest Advances in Materials, Fabrication Techniques, and Stability Enhancement Strategies, *Micromachines*, 2024, **15**(2), 192, DOI: 10.3390/mi15020192.

22 M. Noman, Z. Khan and S. T. Jan, A Comprehensive Review on the Advancements and Challenges in Perovskite Solar Cell Technology, *RSC Adv.*, 2024, **14**(8), 5085–5131, DOI: 10.1039/D3RA07518D.

23 X. Yang, Q. Gao, Z. Zhao, Y. Guo, Y. Guo, L. Wang, Y. Wang and W. Zhan, Surface Tuning of Noble Metal Doped Perovskite Oxide by Synergistic Effect of Thermal Treatment and Acid Etching: A New Path to High-Performance Catalysts for Methane Combustion, *Appl. Catal., B*, 2018, **239**, 373–382, DOI: 10.1016/j.apcatb.2018.08.038.

24 B.-J. Kim, E. Fabbri, D. F. Abbott, X. Cheng, A. H. Clark, M. Nachtegaal, M. Borlaf, I. E. Castelli, T. Graule and T. J. Schmidt, Functional Role of Fe-Doping in Co-Based Perovskite Oxide Catalysts for Oxygen Evolution Reaction, *J. Am. Chem. Soc.*, 2019, **141**(13), 5231–5240, DOI: 10.1021/jacs.8b12101.

25 M. A. Salguero Salas, J. M. De Paoli, O. E. Linarez Pérez, N. Bajales and V. C. Fuertes, Synthesis and Characterization of Alumina-Embedded SrCo0.95V0.05O3 Nanostructured Perovskite: An Attractive Material for Supercapacitor Devices, *Microporous Mesoporous Mater.*, 2020, **293**, 109797, DOI: 10.1016/j.micromeso.2019.109797.

26 H. Geng, X. Zou, Y. Min, Y. Bu and Q. Lu, Advances and Challenges in Perovskite Oxide Design for High-Performance Zinc–Air Batteries: Integrating Experimental Strategies and Machine Learning, *Adv. Funct. Mater.*, 2025, **10**, 2500657, DOI: 10.1002/adfm.202500657.

27 L. C. C. B. Oliveira, R. Venâncio, P. V. F. de Azevedo, C. G. Anchieta, T. C. M. Nepel, C. B. Rodella, H. Zanin and G. Doubek, *J. Energy Chem.*, 2023, **81**, 1–19.

28 Y. Shao, M. F. El-Kady, J. Sun, Y. Li, Q. Zhang, M. Zhu, H. Wang, B. Dunn and R. B. Kaner, Design and Mechanisms of Asymmetric Supercapacitors, *Chem. Rev.*, 2018, **118**(18), 9233–9280, DOI: 10.1021/acs.chemrev.8b00252.

29 Z. Yu, B. Duong, D. Abbitt and J. Thomas, Highly Ordered MnO_2 Nanopillars for Enhanced Supercapacitor Performance, *Adv. Mater.*, 2013, **25**(24), 3302–3306, DOI: 10.1002/adma.201300572.

30 W. Che, M. Wei, Z. Sang, Y. Ou, Y. Liu and J. Liu, Perovskite LaNiO3-δ Oxide as an Anion-Intercalated Pseudocapacitor Electrode, *J. Alloys Compd.*, 2018, **731**, 381–388, DOI: 10.1016/j.jallcom.2017.10.027.

31 Y. Zhang, J. Ding, W. Xu, M. Wang, R. Shao, Y. Sun and B. Lin, Mesoporous LaFeO3 Perovskite Derived from MOF Gel for All-Solid-State Symmetric Supercapacitors, *Chem. Eng. J.*, 2020, **386**, 124030, DOI: 10.1016/j.cej.2020.124030.

32 X. Dai, C. Yu, R. Li, Q. Wu, K. Shi and Z. Hao, Effect of calcination temperature and reaction conditions on methane partial oxidation using lanthanum-based perovskite as oxygen donor, *J. Rare Earths*, 2008, **26**, 341.

33 Y. Liu, J. Dinh, M. O. Tade and Z. Shao, Design of Perovskite Oxides as Anion-Intercalation-Type Electrodes for Supercapacitors: Cation Leaching Effect, *ACS Appl. Mater. Interfaces*, 2016, **8**(36), 23774–23783, DOI: 10.1021/acsami.6b08634.

34 A. K. Tomar, A. Joshi, G. Singh and R. K. Sharma, Triple Perovskite Oxide as an Advanced Pseudocapacitive Material: Multifarious Element Approach with an Ordered Structure, *J. Mater. Chem. A*, 2020, **8**(45), 24013–24023, DOI: 10.1039/D0TA08995H.

35 G. Nallamuthu, S. Thangavel, K. Kirubakaran, V. Vasudevan, Y. Sivalingam and G. Venugopal, Study of Structural and Electrochemical Properties of La2SrV2O9 Perovskites Prepared Using Ball-Milling, *Appl. Surf. Sci.*, 2018, **449**, 468–473, DOI: 10.1016/j.apsusc.2017.12.187.

36 Y. Liu, Z. Wang, J. M. Veder, Z. Xu, Y. Zhong, W. Zhou, M. O. Tade, S. Wang and Z. Shao, Highly Defective Layered Double Perovskite Oxide for Efficient Energy Storage via Reversible Pseudocapacitive Oxygen-Anion

Intercalation, *Adv. Energy Mater.*, 2018, **8**(11), 1702604, DOI: 10.1002/aenm.201702604.

37 M. Rudra, H. S. Tripathi, A. Dutta and T. P. Sinha, Existence of Nearest-Neighbor and Variable Range Hopping in Pr2ZnMnO6 Oxygen-Intercalated Pseudocapacitor Electrode, *Mater. Chem. Phys.*, 2021, **258**, 123907, DOI: 10.1016/j.matchemphys.2020.123907.

38 J. Shi and L. Guo, ABO3-Based Photocatalysts for Water Splitting, *Prog. Nat. Sci.:Mater. Int.*, 2012, **22**(6), 592–615, DOI: 10.1016/j.pnsc.2012.12.002.

39 B. Levasseur and S. Kaliaguine, Methanol oxidation on $LaBO_3$ (B = Co, Mn, Fe) perovskite-type catalysts prepared by reactive grinding, *Appl. Catal., A*, 2008, **343**, 29.

40 L. C. C. B. Oliveira, R. Venâncio, P. V. F. de Azevedo, C. G. Anchieta, T. C. M. Nepel, C. B. Rodella, H. Zanin and G. Doubek, Reviewing Perovskite Oxide Sites Influence on Electrocatalytic Reactions for High Energy Density Devices, *J. Energy Chem.*, 2023, **81**, 1–19, DOI: 10.1016/j.jechem.2023.02.013.

41 E. Grabowska, Selected Perovskite Oxides: Characterization, Preparation and Photocatalytic Properties—A Review, *Appl. Catal., B*, 2016, **186**, 97–126, DOI: 10.1016/j.apcatb.2015.12.035.

42 E. A. R. Assirey, Perovskite Synthesis, Properties and Their Related Biochemical and Industrial Application, *Saudi Pharm. J.*, 2019, **27**(6), 817–829, DOI: 10.1016/j.jsps.2019.05.003.

43 S. Vasala and M. Karppinen, A2B′B″O6 Perovskites: A Review, *Prog. Solid State Chem.*, 2015, **43**(1–2), 1–36, DOI: 10.1016/j.progsolidstchem.2014.08.001.

44 H. J. Song, H. Yoon, B. Ju and D. Kim, Highly Efficient Perovskite-Based Electrocatalysts for Water Oxidation in Acidic Environments: A Mini Review, *Adv. Energy Mater.*, 2021, **11**(27), 2002428, DOI: 10.1002/aenm.202002428.

45 M. Lebid and M. Omari, Synthesis and Electrochemical Properties of $LaFeO_3$ Oxides Prepared Via Sol–Gel Method, *Arabian J. Sci. Eng.*, 2014, **39**, 147–152, DOI: 10.1007/s13369-013-0883-8.

46 E. K. Albrecht and A. J. Karttunen, Investigation on the Predictive Power of Tolerance Factor τ for A-Site Double Perovskite Oxides, *Dalton Trans.*, 2023, **52**(35), 12461–12469, DOI: 10.1039/D3DT01990J.

47 S. Jana, P. Aich, P. A. Kumar, O. K. Forslund, E. Nocerino, V. Pomjakushin, M. Månsson, Y. Sassa, P. Svedlindh, O. Karis, V. Siruguri and S. Ray, Revisiting Goodenough-Kanamori Rules in a New Series of Double Perovskites LaSr1−xCaxNiReO6, *Sci. Rep.*, 2019, **9**(1), 18296, DOI: 10.1038/s41598-019-54427-0.

48 N. S. Rogado, J. Li, A. W. Sleight and M. A. Subramanian, Magnetocapacitance and Magnetoresistance Near Room Temperature in a Ferromagnetic Semiconductor: La_2NiMnO_6, *Adv. Mater.*, 2005, **17**(18), 2225–2227, DOI: 10.1002/adma.200500737.Cr.

49 L. Chen, J. Ding and X. Zhu, A Review on Research Progress of Double Perovskite Oxides for Oxygen Evolution Reaction Electrocatalysts and Supercapacitors, *RSC Appl. Interfaces*, 2025, **2**(2), 320–351, DOI: 10.1039/D4LF00395K.

50 T. Maiti, M. Saxena and P. Roy, Double Perovskite ($Sr_2B'B''O_6$) Oxides for High-Temperature Thermoelectric Power Generation—A Review, *J. Mater. Res.*, 2019, **34**(1), 107–125, DOI: 10.1557/jmr.2018.376.

51 B. Bochu, M. N. Deschizeaux, J. C. Joubert, A. Collomb, J. Chenavas and M. Marezio, Synthèse et caractérisation d'une série de titanates pérowskites isotypes de $[CaCu_0](Mn_4)O_{12}$, *J. Solid State Chem.*, 1979, **29**, 291–298.

52 C. Meyer, S. Hühn, M. Jungbauer, S. Merten, B. Damaschke, K. Samwer and V. Moshnyaga, Tip-enhanced Raman Spectroscopy (TERS) on Double Perovskite La_2CoMnO_6 Thin Films: Field Enhancement and Depolarization Effects, *J. Raman Spectrosc.*, 2017, **48**(1), 46–52, DOI: 10.1002/jrs.4986.

53 S. Aftab, X. Li, F. Kabir, E. Akman, M. Aslam, M. R. Pallavolu, G. Koyyada, M. A. Assiri and A. H. Rajpar, Lighting the Future: Perovskite Nanorods and Their Advances across Applications, *Nano Energy*, 2024, **124**, 109504, DOI: 10.1016/j.nanoen.2024.109504.

54 K. Shigematsu, K. Shimizu, K. Yamamoto, T. Nishikubo, Y. Sakai, S. A. Nikolaev, H. Das and M. Azuma, Strain Manipulation of Magnetic Anisotropy in Room-Temperature Ferrimagnetic Quadruple Perovskite $CeCu_3Mn_4O_{12}$, *ACS Appl. Electron. Mater.*, 2019, **1**(12), 2514–2521, DOI: 10.1021/acsaelm.9b00547.

55 L. Gao, X. Wang, X. Ye, W. Wang, Z. Liu, S. Qin, Z. Hu, H.-J. Lin, S.-C. Weng, C.-T. Chen, P. Ohresser, F. Baudelet, R. Yu, C. Jin and Y. Long, Near-Room-Temperature Ferrimagnetic Ordering in a B-Site-Disordered 3d–5d-Hybridized Quadruple Perovskite Oxide, $CaCu_3Mn_2Os_2O_{12}$, *Inorg. Chem.*, 2019, **58**(22), 15529–15535, DOI: 10.1021/acs.inorgchem.9b02576.

56 J. Singh and A. Kumar, Investigation of Structural, Morphological and Electrochemical Properties of Mesoporous La2CuCoO6 Rods Fabricated by Facile Hydrothermal Route, *Int. J. Miner., Metall. Mater.*, 2020, **27**(7), 987–995, DOI: 10.1007/s12613-020-2011-6.

57 A. Kumar, Energy Storage Properties of Double Perovskites Gd2NiMnO6 for Electrochemical Supercapacitor Application, *Solid State Sci.*, 2020, **105**, 106252, DOI: 10.1016/j.solidstatesciences.2020.106252.

58 X. Lang, *et al.*, Ag nanoparticles decorated perovskite La0.85Sr0.15MnO3 as electrode materials for supercapacitors, *Mater. Lett.*, 2019, **243**, 34–37, DOI: 10.1016/j.matlet.2019.02.002.

59 P. Lannelongue, *et al.*, Investigation of Ba0.5Sr0.5CoxFe1-xO3-δ as a pseudocapacitive electrode material with high volumetric capacitance, *Electrochim. Acta*, 2018, **271**, 677–684, DOI: 10.1016/j.electacta.2018.03.173.

60 Z. Meng, J. Xu, P. Yu, X. Hu, Y. Wu, Q. Zhang, Y. Li, L. Qiao, Y. Zeng and H. Tian, Double Perovskite La2CoMnO6 Hollow Spheres Prepared by Template Impregnation for High-Performance Supercapacitors, *Chem. Eng. J.*, 2020, **400**, 125966, DOI: 10.1016/j.cej.2020.125966.

61 S. De, M. M. Kurian, L. Solaiappan, A. Kumar, S. Das, S. Samanta, Y. K. Arafath and S. P. Nagappan Nair, Chemistry and Physics of Triple Perovskite Oxides: A

Topical Review, *Chem. Mater.*, 2024, **36**(19), 9207–9233, DOI: 10.1021/acs.chemmater.4c00603.

62 A. Nag, S. Bhowal, M. M. Sala, A. Efimenko, I. Dasgupta and S. Ray, Hopping-Induced Ground-State Magnetism in 6H Perovskite Iridates, *Phys. Rev. Lett.*, 2019, **123**(1), 017201, DOI: 10.1103/PhysRevLett.123.017201.

63 Y. Qiao, G. Liu, R. Xu, R. Hu, L. Liu, G. Jiang, M. Demir and P. Ma, SrFe1-Zr O3-δ Perovskite Oxides as Negative Electrodes for Supercapacitors, *Electrochim. Acta*, 2023, **437**, 141527, DOI: 10.1016/j.electacta.2022.141527.

64 L. Zhu, Y. Liu, C. Su, W. Zhou, M. Liu and Z. Shao, Perovskite $SrCo_{0.9}Nb_{0.1}O_{3-\delta}$ as an Anion-Intercalated Electrode Material for Supercapacitors with Ultrahigh Volumetric Energy Density, *Angew. Chem.*, 2016, **128**(33), 9728–9731, DOI: 10.1002/ange.201603601.

65 Y. Liu, Z. Wang, Y. Zhong, X. Xu, J.-P. M. Veder, M. R. Rowles, M. Saunders, R. Ran and Z. Shao, Activation-Free Supercapacitor Electrode Based on Surface-Modified Sr2CoMo1-XNixO6-δ Perovskite, *Chem. Eng. J.*, 2020, **390**, 124645, DOI: 10.1016/j.cej.2020.124645.

66 M. R. Imer, L. Suescun and F. A. Rabuffetti, Structure of Triple Perovskite BaSr2MgTa2O9 Revisited, *J. Solid State Chem.*, 2022, **306**, 122710, DOI: 10.1016/j.jssc.2021.122710.

67 P. Tan, M. Liu, Z. Shao and M. Ni, Recent Advances in Perovskite Oxides as Electrode Materials for Nonaqueous Lithium–Oxygen Batteries, *Adv. Energy Mater.*, 2017, **7**(13), 1602674, DOI: 10.1002/aenm.201602674.

68 X. Xu, W. Wang, W. Zhou and Z. Shao, Recent Advances in Novel Nanostructuring Methods of Perovskite Electrocatalysts for Energy-Related Applications, *Small Methods*, 2018, **2**(7), 1800071, DOI: 10.1002/smtd.201800071.

69 R. Selvarajan, S. Vadivel, M. Arivanandhan and R. Jayavel, Facile synthesis of pervoskite type BiYO3 embedded reduced graphene oxide (RGO) composite for supercapacitor applications, *Ceram. Int.*, 2020, **46**(3), 3471–3478, DOI: 10.1016/j.ceramint.2019.10.060.

70 H. Nan, X. Hu and H. Tian, Recent Advances in Perovskite Oxides for Anion-Intercalation Supercapacitor: A Review, *Mater. Sci. Semicond. Process.*, 2019, **94**, 35–50, DOI: 10.1016/j.mssp.2019.01.033.

71 K. Brezesinski, J. Wang, J. Haetge, C. Reitz, S. O. Steinmueller, S. H. Tolbert, B. M. Smarsly, B. Dunn and T. Brezesinski, Pseudocapacitive Contributions to Charge Storage in Highly Ordered Mesoporous Group V Transition Metal Oxides with Iso-Oriented Layered Nanocrystalline Domains, *J. Am. Chem. Soc.*, 2010, **132**(20), 6982–6990, DOI: 10.1021/ja9106385.

72 B. Mendoza-Sánchez and P. S. Grant, Charge Storage Properties of a α-MoO3/Carboxyl-Functionalized Single-Walled Carbon Nanotube Composite Electrode in a Li Ion Electrolyte, *Electrochim. Acta*, 2013, **98**, 294–302, DOI: 10.1016/j.electacta.2013.03.072.

73 N. Aristidou, C. Eames, I. Sanchez-Molina, X. Bu, J. Kosco, M. S. Islam and S. A. Haque, Fast Oxygen Diffusion and Iodide Defects Mediate Oxygen-Induced Degradation of Perovskite Solar Cells, *Nat. Commun.*, 2017, **8**(1), 15218, DOI: 10.1038/ncomms15218.

74 J. Prado-Gonjal, D. Ávila, M. E. Villafuerte-Castrejón, F. González-García, L. Fuentes, R. W. Gómez, J. L. Pérez-Mazariego, V. Marquina and E. Morán, Structural, Microstructural and Mössbauer Study of BiFeO3 Synthesized at Low Temperature by a Microwave-Hydrothermal Method, *Solid State Sci.*, 2011, **13**(11), 2030–2036, DOI: 10.1016/j.solidstatesciences.2011.09.006.

75 D. K. Becerra-Paniagua, E. B. Díaz-Cruz, A. Baray-Calderón, A. R. Garcia-Angelmo, E. Regalado-Pérez, M. del Pilar Rodriguez-Torres and C. Martínez-Alonso, Nanostructured Metal Sulphides Synthesized by Microwave-Assisted Heating: A Review, *J. Mater. Sci.: Mater. Electron.*, 2022, **33**(29), 22631–22667, DOI: 10.1007/s10854-022-09024-9.

76 E. M. Kostyukhin, A. L. Kustov and L. M. Kustov, One-step hydrothermal microwave-assisted synthesis of $LaFeO_3$ nanoparticles, *Ceram. Int.*, 2019, **45**, 14384–14388.

77 C. Lin, Z. Lyu, Y. Zhuo, C. Zhao, J. Yang, C. Liu, J. Kim, T. He, L. Hu, F. Li, Y. Shen, K. Liu, W. Yu and T. Wu, Microwave Synthesis and High-Mobility Charge Transport of Carbon-Nanotube-in-Perovskite Single Crystals, *Adv. Opt. Mater.*, 2020, **8**(24), 2001740, DOI: 10.1002/adom.202001740.

78 K. Sumida, K. Liang, J. Reboul, I. A. Ibarra, S. Furukawa and P. Falcaro, Sol–Gel Processing of Metal–Organic Frameworks, *Chem. Mater.*, 2017, **29**(7), 2626–2645, DOI: 10.1021/acs.chemmater.6b03934.

79 J. Moreno, J. M. Dominguez and L. Vicente, Synthesis and characterization of $MTiO_3$(M = Mg, Ca, Sr, Ba) Sol-Gel, *J. Mater. Chem.*, 1995, **5**, 509–512.

80 D. Navas, S. Fuentes, A. Castro-Alvarez and E. Chavez-Angel, Review on Sol-Gel Synthesis of Perovskite and Oxide Nanomaterials, *Gels*, 2021, **7**(4), 275, DOI: 10.3390/gels7040275.

81 P. R. Kharangarh and G. Singh, Effect of Mo-Doped Strontium Cobaltite on Graphene Nanosheets for Creating a Superior Electrode in Supercapacitor Applications, *ECS J. Solid State Sci. Technol.*, 2023, **12**(3), 031006, DOI: 10.1149/2162-8777/acc095.

82 H. Hu, L. Wu, Y. Tan, Q. Zhong, M. Chen, Y. Qiu, D. Yang, B. Sun, Q. Zhang and Y. Yin, Interfacial Synthesis of Highly Stable $CsPbX_3$/Oxide Janus Nanoparticles, *J. Am. Chem. Soc.*, 2018, **140**(1), 406–412, DOI: 10.1021/jacs.7b11003.

83 Y. Zhang, J. Ding, W. Xu, M. Wang, R. Shao, Y. Sun and B. Lin, Mesoporous LaFeO3 Perovskite Derived from MOF Gel for All-Solid-State Symmetric Supercapacitors, *Chem. Eng. J.*, 2020, **386**, 124030, DOI: 10.1016/j.cej.2020.124030.

84 V. V. Deshmukh, C. R. Ravikumar, M. R. A. Kumar, S. Ghotekar, A. N. Kumar, A. A. Jahagirdar and H. C. A. Murthy, Structure, Morphology and Electrochemical Properties of SrTiO3 Perovskite: Photocatalytic and Supercapacitor Applications, *Environ. Chem. Ecotoxicol.*, 2021, **3**, 241–248, DOI: 10.1016/j.enceco.2021.07.001.

85 A. K. Tomar, G. Singh and R. K. Sharma, Charge Storage Characteristics of Mesoporous Strontium Titanate

Perovskite Aqueous as Well as Flexible Solid-State Supercapacitor Cell, *J. Power Sources*, 2019, **426**, 223–232, DOI: 10.1016/j.jpowsour.2019.04.049.

86 A. Shereef, J. Kunjumon, A. K. Jose, P. A. Aleena, M. Tomy, W. Akram, R. P. Jebin, T. S. Xavier, T. Maity and D. Sajan, Synthesis, Magnetic Properties, and Electrochemical Evaluation of La2NiMnO6 Double Perovskite as Electrode Materials for Supercapacitor Applications, *Ceram. Int.*, 2024, **50**(9), 15756–15766, DOI: 10.1016/j.ceramint.2024.02.056.

87 A. Shereef, A. K. Jose, J. Kunjumon, P. A. Aleena, M. A. Anu, W. Akram, R. P. Jebin, T. S. Xavier, T. Maity and D. Sajan, Study on Preparation, Magnetic Properties and Performance of Electrochemical Supercapacitor Based on La2FeMnO6 Double Perovskite for Energy Storage Applications and Their Charge Storage Mechanism, *Adv. Powder Technol.*, 2024, **35**(9), 104618, DOI: 10.1016/j.apt.2024.104618.

88 L. Ndlwana, N. Raleie, K. M. Dimpe, H. F. Ogutu, E. O. Oseghe, M. M. Motsa, T. A. M. Msagati and B. B. Mamba, Sustainable Hydrothermal and Solvothermal Synthesis of Advanced Carbon Materials in Multidimensional Applications: A Review, *Materials*, 2021, **14**(17), 5094, DOI: 10.3390/ma14175094.

89 M. Riaz, T. Munawar, M. S. Nadeem, F. Mukhtar, S. D. Ali, S. Manzoor, M. N. Ashiq and F. Iqbal, Facile Synthesis of Fullerene-C60 and RGO-Supported KCdCl3-Based Halide Perovskite Nanocomposites toward Effective Electrode Material for Supercapacitor, *J. Appl. Electrochem.*, 2023, **53**(4), 673–687, DOI: 10.1007/s10800-022-01809-4.

90 N. Hussain, F. Wu, W. Younas and L. Xu, Hollow Sphere Formation by the Self Aggregation of Perovskite Fluoride $NaNiF_3$ Nanocrystals and the Application of These Spheres as an Electrode in an Ultrahigh Performance Asymmetric Supercapacitor, *New J. Chem.*, 2019, **43**(30), 11959–11967, DOI: 10.1039/C9NJ02221J.

91 N. Bibi, M. Z. Hussain, S. Hussain, S. Ahmed, I. Ahmad, S. Zhang and A. Iqbal, Excellent Electrochemical Performance of SrZrO3 Nanorods as Supercapacitor Electrode in Aqueous Electrolytes, *Appl. Surf. Sci.*, 2019, **495**, 143587, DOI: 10.1016/j.apsusc.2019.143587.

92 U. M. Patil, K. V. Gurav, O.-S. Joo and C. D. Lokhande, Synthesis of Photosensitive Nanograined TiO2 Thin Films by SILAR Method, *J. Alloys Compd.*, 2009, **478**(1–2), 711–715, DOI: 10.1016/j.jallcom.2008.11.160.

93 Z.-C. Tseng, Y.-Y. Jiang, C.-Y. Lin, J.-Y. Do, T.-H. Hsu, C.-W. Shih, Y.-Z. Chang, S.-Y. Liao and C.-Y. Huang, Highly Stable Flexible Ozone Gas Sensors Using Mn3O4 Nanoparticles-Decorated IGZO Thin Films through the SILAR Method, *Ceram. Int.*, 2024, **50**(16), 28584–28592, DOI: 10.1016/j.ceramint.2024.05.168.

94 I. Dursun, M. De Bastiani, B. Turedi, B. Alamer, A. Shkurenko, J. Yin, A. M. El-Zohry, I. Gereige, A. AlSaggaf, O. F. Mohammed, M. Eddaoudi and O. M. Bakr, *ChemSusChem*, 2017, **10**, 3746.

95 Y. F. Nicolau, Solution deposition of thin solid compound films by a successive ionic-layer adsorption and reaction process, *Appl. Surf. Sci.*, 1985, **22–23**, 1061–1074.

96 M. Yasmeen, S. A. Batool, S. I. A. Shah, M. N. Ashiq, M. Atiq ur Rehman, A. Khaliq, T. Subhani, M. Ramadan and M. A. Basit, Effective Development and Utilization of SILAR-Assisted TiO2 and CsPb2Br5 Nanocomposites for Photochemical and Biological Cleaning of Environment, *Ceram. Int.*, 2024, **50**(12), 21253–21264, DOI: 10.1016/j.ceramint.2024.03.234.

97 S. A. Mane, A. V. Moholkar and A. V. Ghule, A Green Approach for Synthesis of an Efficient Nano Pebbles-like BiVO4@C Electrode for Supercapacitor Application, *Next Mater.*, 2023, **1**(4), 100045, DOI: 10.1016/j.nxmate.2023.100045.

98 M. S. Islam, B. C. Ang, A. Andriyana and A. M. Afifi, A Review on Fabrication of Nanofibers via Electrospinning and Their Applications, *SN Appl. Sci.*, 2019, **1**(10), 1248, DOI: 10.1007/s42452-019-1288-4.

99 Y. Cao, B. Lin, Y. Sun, H. Yang and X. Zhang, Sr-Doped Lanthanum Nickelate Nanofibers for High Energy Density Supercapacitors, *Electrochim. Acta*, 2015, **174**, 41–50, DOI: 10.1016/j.electacta.2015.05.131.

100 G. George, S. L. Jackson, C. Q. Luo, D. Fang, D. Luo, D. Hu, J. Wen and Z. Luo, Effect of Doping on the Performance of High-Crystalline SrMnO3 Perovskite Nanofibers as a Supercapacitor Electrode, *Ceram. Int.*, 2018, **44**(17), 21982–21992, DOI: 10.1016/j.ceramint.2018.08.313.

101 A. Roy, F. E. Cancino-Gordillo, S. Saha, U. Pal and S. Das, Performance of Asymmetric Supercapacitor Fabricated with Perovskite-type Sr^{2+} -incorporated $LaMnO_3$ ($La_{0.7}Sr_{0.3}MnO_3$) Nanostructures in Neutral 1M Na_2SO_4 Aqueous Electrolyte, *Int. J. Energy Res.*, 2021, **45**(9), 14021–14033, DOI: 10.1002/er.6727.

102 X. W. Wang, Q. Q. Zhu, X. E. Wang, H. C. Zhang, J. J. Zhang and L. F. Wang, Structural and Electrochemical Properties of La0.85Sr0.15MnO3 Powder as an Electrode Material for Supercapacitor, *J. Alloys Compd.*, 2016, **675**, 195–200, DOI: 10.1016/j.jallcom.2016.03.048.

103 X. Lang, H. Mo, X. Hu and H. Tian, Supercapacitor Performance of Perovskite $La_{1-x}Sr_xMnO_3$, *Dalton Trans.*, 2017, **46**(40), 13720–13730, DOI: 10.1039/C7DT03134C.

104 Y. Cao, J. Liang, X. Li, L. Yue, Q. Liu, S. Lu, A. M. Asiri, J. Hu, Y. Luo and X. Sun, Recent Advances in Perovskite Oxides as Electrode Materials for Supercapacitors, *Chem. Commun.*, 2021, **57**(19), 2343–2355, DOI: 10.1039/D0CC07970G.

105 A. K. Tomar, G. Singh and R. K. Sharma, Fabrication of a Mo-Doped Strontium Cobaltite Perovskite Hybrid Supercapacitor Cell with High Energy Density and Excellent Cycling Life, *ChemSusChem*, 2018, **11**(23), 4123–4130, DOI: 10.1002/cssc.201801869.

106 J. T. Mefford, W. G. Hardin, S. Dai, K. P. Johnston and K. J. Stevenson, Anion Charge Storage through Oxygen Intercalation in LaMnO3 Perovskite Pseudocapacitor Electrodes, *Nat. Mater.*, 2014, **13**(7), 726–732, DOI: 10.1038/nmat4000.

107 Y. Qian, Q. Ruan, M. Xue and L. Chen, Emerging Perovskite Materials for Supercapacitors: Structure, Synthesis, Modification, Advanced Characterization, Theoretical Calculation and Electrochemical Performance, *J. Energy Chem.*, 2024, **89**, 41–70, DOI: **10.1016/j.jechem.2023.10.028**.

108 K. Chu, W. Zong, G. Xue, H. Guo, J. Qin, H. Zhu, N. Zhang, Z. Tian, H. Dong, Y.-E. Miao, M. B. J. Roeffaers, J. Hofkens, F. Lai and T. Liu, Cation Substitution Strategy for Developing Perovskite Oxide with Rich Oxygen Vacancy-Mediated Charge Redistribution Enables Highly Efficient Nitrate Electroreduction to Ammonia, *J. Am. Chem. Soc.*, 2023, **145**(39), 21387–21396, DOI: **10.1021/jacs.3c06402**.

109 J. He, Y. Zhou, S. Wu, J. Cao, B. Han, Z. Wang, Z. Tong, M. Demir and P. Ma, Unlocking the Capacity and Stability Limitations of Perovskite Electrodes and Achieving the Design of a Flame-Retardant Supercapacitor Through the "Tree Canopy" Structure, *ACS Energy Lett.*, 2025, **10**(4), 1680–1687, DOI: **10.1021/acsenergylett.5c00154**.

110 N. P. D. Ngidi, A. F. Koekemoer and S. S. Ndlela, Recent Advancement in the Electrochemical Performance of Electrochemical Capacitors Based on Biomass-Derived Porous Carbon: A Review, *J. Energy Storage*, 2024, **89**, 111638, DOI: **10.1016/j.est.2024.111638**.

111 Y. Liu, S. P. Jiang and Z. Shao, Intercalation Pseudocapacitance in Electrochemical Energy Storage: Recent Advances in Fundamental Understanding and Materials Development, *Mater. Today Adv.*, 2020, **7**, 100072, DOI: **10.1016/j.mtadv.2020.100072**.

112 D. S. Sawant, S. V. Gaikwad, A. V. Fulari, M. Govindasamy, S. B. Kulkarni, D. P. Dubal and G. M. Lohar, Theoretical Specific Capacity and Metal Ion Diffusion Pathway of $NiMoO_4$ Microspheres for Hybrid Supercapacitors, *Small*, 2025, **21**(13), 2500080, DOI: **10.1002/smll.202500080**.

113 X. Yang, A. J. Fernández-Carrión, X. Geng and X. Kuang, B-Site Deficient Hexagonal Perovskites: Structural Stability, Ionic Order-Disorder and Electrical Properties, *Prog. Solid State Chem.*, 2024, **74**, 100459, DOI: **10.1016/j.progsolidstchem.2024.100459**.

114 Y. Li, N. Mushtaq, Y. Chen, W. Ye, Z. Zhuang, M. Singh, Y. Jing and L. Fan, Revisiting Mo-Doped $SrFeO_{3-\delta}$ Perovskite: The Origination of Cathodic Activity and Longevity for Intermediate-Temperature Solid Oxide Fuel Cells, *Adv. Funct. Mater.*, 2025, **35**(3), 2411025, DOI: **10.1002/adfm.202411025**.

115 A. M. Teli, S. A. Beknalkar, R. U. Amte, P. J. Morankar, M. A. Yewale, V. V. Burungale, C.-W. Jeon, H. Efstathiadis and J. C. Shin, Investigating into the Intricacies of Charge Storage Kinetics in NbMn-Oxide Composite Electrodes for Asymmetric Supercapacitor and HER Applications, *J. Alloys Compd.*, 2023, **965**, 171305, DOI: **10.1016/j.jallcom.2023.171305**.

116 Li, J. Sunarso, Y. Yang, Y. Chen, C. Ge, W. Wang, Y. Guo, R. Ran and W. Zhou, Strategies for improving oxygen ionic conducting in perovskite oxides and their practical applications, *Energy Rev.*, 2024, **3**, 100085, DOI: **10.1016/j.enrev.2024.100085**.

117 O. B. Okafor, A. P. I. Popoola, O. M. Popoola and S. O. Adeosun, Review on the Recent Development on Polyaniline and Transition Metal Oxides Composite Electrode for Supercapacitor Application, *Next Mater.*, 2025, **6**, 100389, DOI: **10.1016/j.nxmate.2024.100389**.

118 Y. Pathaare, A. M. Reddy, P. Sangrulkar, B. Kandasubramanian and A. Satapathy, Carbon Hybrid Nano-Architectures as an Efficient Electrode Material for Supercapacitor Applications, *Hybrid Adv.*, 2023, **3**, 100041, DOI: **10.1016/j.hybadv.2023.100041**.

119 S. Soleimani, K. Pishvaie and M. Saidi, Perovskite Oxides as Promising Candidates for Advanced Supercapacitor Electrode Materials: A Review, *J. Power Sources*, 2025, **640**, 236760, DOI: **10.1016/j.jpowsour.2025.236760**.

120 Z. Jia, C. Cheng, X. Chen, L. Liu, R. Ding, J. Ye, J. Wang, L. Fu, Y. Cheng and Y. Wu, Applications of All-Inorganic Perovskites for Energy Storage, *Mater. Adv.*, 2023, **4**(1), 79–104, DOI: **10.1039/D2MA00779G**.

121 D. Navas, S. Fuentes, A. Castro-Alvarez and E. Chavez-Angel, Review on Sol-Gel Synthesis of Perovskite and Oxide Nanomaterials, *Gels*, 2021, **7**(4), 275, DOI: **10.3390/gels7040275**.

122 W. Azouzi, W. Sigle, H. Labrim and M. Benaissa, Sol-Gel Synthesis of Nanoporous LaFeO3 Powders for Solar Applications, *Mater. Sci. Semicond. Process.*, 2019, **104**, 104682, DOI: **10.1016/j.mssp.2019.104682**.

123 M. S. Akhtar, I. H. Gul, M. M. Baig and M. A. Akram, Binder-Free Pseudocapacitive Nickel Cobalt Sulfide/MWCNTs Hybrid Electrode Directly Grown on Nickel Foam for High Rate Supercapacitors, *Mater. Sci. Eng., B*, 2021, **264**, 114898, DOI: **10.1016/j.mseb.2020.114898**.

124 W. Wu, X. Wang, X. Wang, F. Li, T. Xu and X. Li, Nanoflower-like Cu2CoSnS4 Grown on Nickel Foam as Binder-Free Electrode Material for Asymmetric Supercapacitors with High Rate and Capacitance, *J. Alloys Compd.*, 2023, **947**, 169590, DOI: **10.1016/j.jallcom.2023.169590**.

125 W.-C. Chen, C.-C. Hu, C.-C. Wang and C.-K. Min, Electrochemical Characterization of Activated Carbon–Ruthenium Oxide Nanoparticles Composites for Supercapacitors, *J. Power Sources*, 2004, **125**(2), 292–298, DOI: **10.1016/j.jpowsour.2003.08.001**.

126 E. A. R. Assirey, Perovskite Synthesis, Properties and Their Related Biochemical and Industrial Application, *Saudi Pharm. J.*, 2019, **27**(6), 817–829, DOI: **10.1016/j.jsps.2019.05.003**.

127 A. S. R. Bati, Y. L. Zhong, P. L. Burn, M. K. Nazeeruddin, P. E. Shaw and M. Batmunkh, Next-Generation Applications for Integrated Perovskite Solar Cells, *Commun. Mater.*, 2023, **4**(1), 2, DOI: **10.1038/s43246-022-00325-4**.

128 Z. Li, X. Mao, D. Feng, *et al.*, Prediction of perovskite oxygen vacancies for oxygen electrocatalysis at different temperatures, *Nat. Commun.*, 2024, **15**, 9318, DOI: **10.1038/s41467-024-53578-7**.

129 X. Lang, H. Zhang, X. Xue, C. Li, X. Sun, Z. Liu, H. Nan, X. Hu and H. Tian, Rational Design of

La0.85Sr0.15MnO3@NiCo2O4 Core–Shell Architecture Supported on Ni Foam for High Performance Supercapacitors, *J. Power Sources*, 2018, **402**, 213–220, DOI: 10.1016/j.jpowsour.2018.09.040.

130 N. F. Atta, A. Galal and E. H. El-Ads, Perovskite Nanomaterials – Synthesis, Characterization, and Applications, in *Perovskite Materials – Synthesis, Characterisation, Properties, and Applications*, InTech, 2016, DOI: 10.5772/61280.

131 M. Girirajan, A. K. Bojarajan, I. N. Pulidindi, K. N. Hui and S. Sangaraju, An Insight into the Nanoarchitecture of Electrode Materials on the Performance of Supercapacitors, *Coord. Chem. Rev.*, 2024, **518**, 216080, DOI: 10.1016/j.ccr.2024.216080.

132 M. Habibi, H. Sohrabi and M. Reza Majidi, Towards High-Performance Perovskite-Based Supercapacitors: A Review of Recent Research Developments, *Mater. Sci. Eng., B*, 2025, **317**, 118110, DOI: 10.1016/j.mseb.2025.118110.

133 N. Lei, P. Ma, B. Yu, S. Li, J. Dai and G. Jiang, Anion-Intercalated Supercapacitor Electrode Based on Perovskite-Type SrB0.875Nb0.125O3 (B = Mn, Co), *Chem. Eng. J.*, 2021, **421**, 127790, DOI: 10.1016/j.cej.2020.127790.

134 C. I. Priyadharsini, G. Marimuthu, T. Pazhanivel, P. M. Anbarasan, V. Aroulmoji, S. Prabhu and R. Ramesh, Electrochemical Supercapacitor Studies of Ni2+-Doped SrTiO3 Nanoparticles by a Ball Milling Method, *Ionics*, 2020, **26**(7), 3591–3597, DOI: 10.1007/s11581-019-03412-8.

135 M. Ramesh, V. Viswanath N, J. Yesuraj, K. Kim and K. Biswas, RETRACTED: Oxygen Vacancy Induced High Specific Capacitance in Sr2CoSbO6, *Mater. Sci. Semicond. Process.*, 2022, **148**, 106806, DOI: 10.1016/j.mssp.2022.106806.

136 M. Ahangari, E. Mahmoodi, N. Delibaş, J. Mostafaei, E. Asghari and A. Niaei, Application of SrFeO3 Perovskite as Electrode Material for Supercapacitor and Investigation of Co-Doping Effect on the B-Site, *Turk. J. Chem.*, 2022, **46**(5), 1723–1732, DOI: 10.55730/1300-0527.3475.

137 V. Celorrio, A. S. Leach, H. Huang, S. Hayama, A. Freeman, D. W. Inwood, D. J. Fermin and A. E. Russell, Relationship between Mn Oxidation State Changes and Oxygen Reduction Activity in (La,Ca)MnO_3 as Probed by *In Situ* XAS and XES, *ACS Catal.*, 2021, **11**(11), 6431–6439, DOI: 10.1021/acscatal.1c00997.

138 Y. Zhang, J. Ding, W. Xu, M. Wang, R. Shao, Y. Sun and B. Lin, Mesoporous LaFeO3 Perovskite Derived from MOF Gel for All-Solid-State Symmetric Supercapacitors, *Chem. Eng. J.*, 2020, **386**, 124030, DOI: 10.1016/j.cej.2020.124030.

139 J. Singh, A. Kumar and A. Kumar, Facile Solvothermal Synthesis of Nano-Assembled Mesoporous Rods of Cobalt Free – La2NiFeO6 for Electrochemical Behaviour, *Mater. Sci. Eng., B*, 2020, **261**, 114664, DOI: 10.1016/j.mseb.2020.114664.

140 C. T. Alexander, J. T. Mefford, J. Saunders, R. P. Forslund, K. P. Johnston and K. J. Stevenson, Anion-Based Pseudocapacitance of the Perovskite Library $La_{1-x}Sr_xBO_{3-\delta}$ (B = Fe, Mn, Co), *ACS Appl. Mater. Interfaces*, 2019, **11**(5), 5084–5094, DOI: 10.1021/acsami.8b19592.

141 K. Upendranath, R. S. Vishwanath, G. Ravitheja, A. R. Lamani, G. Sriram, T. H. Oh, M. D. Kurkuri and T. Altalhi, Sol-gel synthesis of LaFeO3 perovskite oxide for distinct ridges detection of level II and III latent fingerprints, *Inorg. Chem. Commun.*, 2024, **170**, 113210, DOI: 10.1016/j.matlet.2019.05.090.

142 X. Lang, H. Zhang, X. Xue, C. Li, X. Sun, Z. Liu, H. Nan, X. Hu and H. Tian, Rational Design of La0.85Sr0.15MnO3@NiCo2O4 Core–Shell Architecture Supported on Ni Foam for High Performance Supercapacitors, *J. Power Sources*, 2018, **402**, 213–220, DOI: 10.1016/j.jpowsour.2018.09.040.

143 P. M. Shafi, N. Nisar and A. C. Bose, One-Pot Synthesis of $LaMnO_3/Mn_3O_4$ Nanocomposite: Impact of Calcination Temperature on the Synergetic Effect Towards High Energy Supercapacitor Performance, *ChemistrySelect*, 2018, **3**(23), 6459–6467, DOI: 10.1002/slct.201800876.

144 X. Lang, H. Mo, X. Hu and H. Tian, Supercapacitor Performance of Perovskite $La_{1-x}Sr_xMnO_3$, *Dalton Trans.*, 2017, **46**(40), 13720–13730, DOI: 10.1039/C7DT03134C.

145 W. Wang, B. Lin, Y. Cao, Y. Sun, X. Zhang, H. Yang and H. Sun, High-performance GdxSr1-xNiO3 porous nanofibers prepared by electrospinning for symmetric and asymmetric supercapacitors, *J. Phys. Chem. Solids*, 2020, **140**, 109361, DOI: 10.1016/j.jpcs.2020.109361.

146 C. T. Alexander, R. P. Forslund, K. P. Johnston and K. J. Stevenson, Tuning Redox Transitions via the Inductive Effect in $LaNi_{1-x}Fe_xO_{3-\delta}$ Perovskites for High-Power Asymmetric and Symmetric Pseudocapacitors, *ACS Appl. Energy Mater.*, 2019, **2**(9), 6558–6568, DOI: 10.1021/acsaem.9b01117.

147 Q. Hu, B. Yue, H. Shao, F. Yang, J. Wang, Y. Wang and J. Liu, Facile Syntheses of Perovskite Type LaMO3 (M=Fe, Co, Ni) Nanofibers for High Performance Supercapacitor Electrodes and Lithium-Ion Battery Anodes, *J. Alloys Compd.*, 2021, **852**, 157002, DOI: 10.1016/j.jallcom.2020.157002.

148 J. Singh, A. Kumar, U. K. Goutam and A. Kumar, Microstructure and Electrochemical Performance of La2ZnMnO6 Nanoflakes Synthesized by Facile Hydrothermal Route, *Appl. Phys. A*, 2020, **126**(1), 11, DOI: 10.1007/s00339-019-3195-3.

149 J. Singh, U. K. Goutam and A. Kumar, Hydrothermal Synthesis and Electrochemical Performance of Nanostructured Cobalt Free La2CuMnO6, *Solid State Sci.*, 2019, **95**, 105927, DOI: 10.1016/j.solidstatesciences.2019.06.016.

150 J. Singh and A. Kumar, Facile Wet Chemical Synthesis and Electrochemical Behavior of La2FeCoO6 Nano-Crystallites, *Mater. Sci. Semicond. Process.*, 2019, **99**, 8–13, DOI: 10.1016/j.mssp.2019.04.007.

151 Z. Meng, J. Xu, P. Yu, X. Hu, Y. Wu, Q. Zhang, Y. Li, L. Qiao, Y. Zeng and H. Tian, Double Perovskite La2CoMnO6 Hollow Spheres Prepared by Template Impregnation for High-Performance Supercapacitors, *Chem. Eng. J.*, 2020, **400**, 125966, DOI: 10.1016/j.cej.2020.125966.

152 H. Mo, H. Nan, X. Lang, S. Liu, L. Qiao, X. Hu and H. Tian, Influence of Calcium Doping on Performance of LaMnO3 Supercapacitors, *Ceram. Int.*, 2018, **44**(8), 9733–9741, DOI: 10.1016/j.ceramint.2018.02.205.

153 Z. Li, W. Zhang, H. Wang and B. Yang, Two-Dimensional Perovskite LaNiO3 Nanosheets with Hierarchical Porous Structure for High-Rate Capacitive Energy Storage, *Electrochim. Acta*, 2017, **258**, 561–570, DOI: 10.1016/j.electacta.2017.11.099.

154 W. Wang, B. Lin, H. Zhang, Y. Sun, X. Zhang and H. Yang, Synthesis, Morphology and Electrochemical Performances of Perovskite-Type Oxide LaxSr1-XFeO3 Nanofibers Prepared by Electrospinning, *J. Phys. Chem. Solids*, 2019, **124**, 144–150, DOI: 10.1016/j.jpcs.2018.09.011.

155 J. Singh and A. Kumar, Nanocrystallite Assembled La2CoNiO6 Nanorods Fabricated by Facile Solvothermal Route for Electrochemical Performance, *J. Nanopart. Res.*, 2021, **23**(9), 208, DOI: 10.1007/s11051-021-05318-x.

156 S. Hussain, M. S. Javed, N. Ullah, A. Shaheen, N. Aslam, I. Ashraf, Y. Abbas, M. Wang, G. Liu and G. Qiao, Unique Hierarchical Mesoporous LaCrO3 Perovskite Oxides for Highly Efficient Electrochemical Energy Storage Applications, *Ceram. Int.*, 2019, **45**(12), 15164–15170, DOI: 10.1016/j.ceramint.2019.04.258.

157 M. L. Mokhnatskyi, I. P. Yaremiy, P. I. Kolkovskyi, L. V. Mokhnatska, S. I. Yaremiy, A. I. Kachmar and Kh. P. Cherkach, Promising Cathode Material for Supercapacitors LaFe0.5Cr0.5O3 Perovskite Nanoparticles, *Phys. Chem. Solid State*, 2020, **21**(4), 635–639, DOI: 10.15330/pcss.21.4.635-639.

158 P. Ma, B. Zhu, Na Lei, Y. Liu, B. Yu, Q. Lu, J. Dai, S. Li and G. Jiang, Effect of Sr substitution on structure and electrochemical properties of perovskite-type LaMn0.9Ni0.1O3 nanofibers, *Mater. Lett.*, 2019, **252**, 23–26, DOI: 10.1016/j.matlet.2019.05.090.

159 H. Tian, X. Lang, H. Nan, P. An, W. Zhang, X. Hu and J. Zhang, Nanosheet-Assembled LaMnO3@NiCo2O4 Nanoarchitecture Growth on Ni Foam for High Power Density Supercapacitors, *Electrochim. Acta*, 2019, **318**, 651–659, DOI: 10.1016/j.electacta.2019.06.133.

160 O. J. Dura, P. Rogl, M. Falmbigl, G. Hilscher and E. Bauer, Thermoelectric and magnetic properties of nanocrystalline La0.7Sr0.3CoO3, *J. Appl. Phys.*, 2012, **111**, 063722, DOI: 10.1063/1.3699038.

161 B. Zhang, P. Liu, Z. Li and X. Song, Synthesis of Two-Dimensional Sr-Doped LaNiO3 Nanosheets with Improved Electrochemical Performance for Energy Storage, *Nanomaterials*, 2021, **11**(1), 155, DOI: 10.3390/nano11010155.

162 E. K. Abdel-Khalek, E. A. Mohamed, D. A. Rayan and S. G. Mohamed, The Enhancement of Supercapacitors Performances of LaMnO3±δ Perovskite by Ag-Doping, *Phys. B*, 2021, **615**, 413065, DOI: 10.1016/j.physb.2021.413065.

163 P. Liu, J. Liu, S. Cheng, W. Cai, F. Yu, Y. Zhang, P. Wu and M. Liu, A High-Performance Electrode for Supercapacitors: Silver Nanoparticles Grown on a Porous Perovskite-Type Material La0.7Sr0.3CoO3−δ Substrate, *Chem. Eng. J.*, 2017, **328**, 1–10, DOI: 10.1016/j.cej.2017.06.150.

164 M. P. Harikrishnan and A. C. Bose, *Perovskite Oxide LaCoO3 Electrode as High Performance Pseudocapacitor*, 2019, vol. 22, p. 060001, DOI: 10.1063/1.5093874.

165 G. Guo, K. Ouyang, J. Yu, Y. Liu, S. Feng and M. Wei, Facile Synthesis of $LaCoO_3$ with a High Oxygen Vacancy Concentration by the Plasma Etching Technique for High-Performance Oxygen Ion Intercalation Pseudocapacitors, *ACS Appl. Energy Mater.*, 2020, **3**(1), 300–308, DOI: 10.1021/acsaem.9b01558.

166 X. W. Wang, Q. Q. Zhu, X. E. Wang, H. C. Zhang, J. J. Zhang and L. F. Wang, Structural and Electrochemical Properties of La0.85Sr0.15MnO3 Powder as an Electrode Material for Supercapacitor, *J. Alloys Compd.*, 2016, **675**, 195–200, DOI: 10.1016/j.jallcom.2016.03.048.

167 W. Yan-Bo, B. Jun and W. Bin-Bin, Preparation and Supercapacitor Properties of Double-Perovskite La_2CoNiO_6 Inorganic Nanofibers, *Acta Phys.-Chim. Sin.*, 2015, **31**(2), 315–321, DOI: 10.3866/PKU.WHXB201412164.

168 B. Zhang, P. Liu, Z. Li and X. Song, Synthesis of Two-Dimensional Sr-Doped LaNiO3 Nanosheets with Improved Electrochemical Performance for Energy Storage, *Nanomaterials*, 2021, **11**(1), 155, DOI: 10.3390/nano11010155.

169 J. Huang, K. Yang, Z. Zhang, L. Yang and S. I. Hirano, Layered perovskite LiEuTiO4 as a 0.8 v lithium intercalation electrode, *Chem. Commun.*, 2017, **53**(55), 7800–7803, DOI: 10.1039/c7cc03933f.

170 R. Mondal, N. K. Mishra, T. Maiyalagan, A. Gupta and P. Singh, $La_{1-x}K_xFeO_{3-\delta}$: An Anion Intercalative Pseudocapacitive Electrode for Supercapacitor Application, *ACS Omega*, 2021, **6**(45), 30488–30498, DOI: 10.1021/acsomega.1c03902.

171 V. Augustyn, P. Simon and B. Dunn, Pseudocapacitive oxide materials for high-rate electrochemical energy storage, *Energy Environ. Sci.*, 2014, **7**(5), 1597–1614, DOI: 10.1039/c3ee44164d.

172 T. Shao, H. You, Z. Zhai, T. Liu, M. Li and L. Zhang, Hollow Spherical LaNiO 3 Supercapacitor Electrode Synthesized by a Facile Template-Free Method, *Mater. Lett.*, 2017, **201**, 122–124, DOI: 10.1016/j.matlet.2017.04.143.

173 S. Nsar, Z. Hassan, K. Y. Cheong and W. Lim, A review on potential use of cerium oxide and doped cerium oxide as high dielectric constant seed layers for overgrowth of cerium oxide nanostructures, *Mater. Res. Express*, 2024, **11**, 062003, DOI: 10.1088/2053-1591/ad52ef.

174 L. Zhu, R. Ran, M. Tadé, W. Wang and Z. Shao, Perovskite Materials in Energy Storage and Conversion, *Asia-Pac. J. Chem. Eng.*, 2016, **11**(3), 338–369, DOI: 10.1002/apj.2000.

175 M. Ahangari, *et al.*, Investigation of structural and electrochemical properties of SrFexCo1-xO3-δ perovskite oxides as a supercapacitor electrode material, *J. Energy Storage*, 2023, **63**, 107034, DOI: 10.1016/j.est.2023.107034.

176 M. P. Harikrishnan, A. J. C. Mary and A. C. Bose, Electrochemical Performance of ANiO3 (A= La, Ce) Perovskite Oxide Material and Its Device Performance for

Supercapattery Application, *Electrochim. Acta*, 2020, **362**, 137095, DOI: 10.1016/j.electacta.2020.137095.

177 S. Rauf, M. B. Hanif, Z. Tayyab, M. Veis, M. A. K. Yousaf Shah, N. Mushtaq, D. Medvedev, Y. Tian, C. Xia, M. Motola and B. Zhu, Alternative Strategy for Development of Dielectric Calcium Copper Titanate-Based Electrolytes for Low-Temperature Solid Oxide Fuel Cells, *Nanomicro Lett.*, 2025, **17**(1), 13, DOI: 10.1007/s40820-024-01523-0.

178 S. Samantaray, P. Mallick, I.-M. Hung, M. Moniruzzaman, S. K. Satpathy and D. Mohanty, Ceramic-Ceramic Nanocomposite Materials for Energy Storage Applications: A Review, *J. Energy Storage*, 2024, **99**, 113330, DOI: 10.1016/j.est.2024.113330.

179 X. Lang, X. Sun, Z. Liu, H. Nan, C. Li, X. Hu and H. Tian, Ag Nanoparticles Decorated Perovskite La0.85Sr0.15MnO3 as Electrode Materials for Supercapacitors, *Mater. Lett.*, 2019, **243**, 34–37, DOI: 10.1016/j.matlet.2019.02.002.

180 G. A. M. Ali, O. A. G. Wahba, A. M. Hassan, O. A. Fouad and K. Feng Chong, Calcium-Based Nanosized Mixed Metal Oxides for Supercapacitor Application, *Ceram. Int.*, 2015, **41**(6), 8230–8234, DOI: 10.1016/j.ceramint.2015.02.100.

181 M. G. Allan, R. A. Yang, S. Marino, M. J. Gordon, P. Christopher and E. Nikolla, Visible Light Photolysis at Single Atom Sites in Semiconductor Perovskite Oxides, *J. Am. Chem. Soc.*, 2025, **147**(1), 898–909, DOI: 10.1021/jacs.4c13821.

182 X. Wang, J. Zhang, Z. Pan, D. Lu, M. Pi, X. Ye, C. Dong, J. Chen, K. Chen, F. Radu, S. Francoual, S. Agrestini, Z. Hu, C.-F. Chang, A. Tanaka, K. Yamaura, Y. Shen and Y. Long, X-Ray Absorption Spectroscopic Study of the Transition-Metal-Only Double Perovskite Oxide Mn_2CoReO_6, *J. Phys. Chem. C*, 2024, **128**(37), 15668–15675, DOI: 10.1021/acs.jpcc.4c04491.

183 X. Zhang, J. Cai, L. Yang, J. Luo, T. Guo and E. Chen, Ligand Strategy for Perovskite Displays: A Review, *ACS Energy Lett.*, 2024, **9**(4), 1587–1603, DOI: 10.1021/acsenergylett.3c02454.

184 I.-H. Yeh, M. Ghobadifard, L. Feng, V. Galievsky and P. V. Radovanovic, Origin of Dopant-Carrier Exchange Coupling and Excitonic Zeeman Splitting in Mn^{2+}-Doped Lead Halide Perovskite Nanocrystals, *Nano Lett.*, 2024, **24**(34), 10554–10561, DOI: 10.1021/acs.nanolett.4c02640.

185 Y. Cao, B. Lin, Y. Sun, H. Yang and X. Zhang, Symmetric/Asymmetric Supercapacitor Based on the Perovskite-Type Lanthanum Cobaltate Nanofibers with Sr-Substitution, *Electrochim. Acta*, 2015, **178**, 398–406, DOI: 10.1016/j.electacta.2015.08.033.

186 J. Lv, Y. Zhang, Z. Lv, X. Huang, Z. Wang, X. Zhu and Bo Wei, Strontium doped lanthanum manganite/manganese dioxide composite electrode for supercapacitor with enhanced rate capability, *Electrochim. Acta*, 2016, **222**, 1585–1591, DOI: 10.1016/j.electacta.2016.11.144.

187 S. Nagamuthu, S. Vijayakumar and K.-S. Ryu, Cerium Oxide Mixed LaMnO3 Nanoparticles as the Negative Electrode for Aqueous Asymmetric Supercapacitor Devices, *Mater. Chem. Phys.*, 2017, **199**, 543–551, DOI: 10.1016/j.matchemphys.2017.07.050.

188 X. Lang, H. Zhang, X. Xue, C. Li, X. Sun, Z. Liu, H. Nan, X. Hu and H. Tian, Rational Design of La0.85Sr0.15MnO3@NiCo2O4 Core–Shell Architecture Supported on Ni Foam for High Performance Supercapacitors, *J. Power Sources*, 2018, **402**, 213–220, DOI: 10.1016/j.jpowsour.2018.09.040.

189 M. D. Stoller, S. Park, Y. Zhu, J. An and R. S. Ruoff, Graphene-Based Ultracapacitors, *Nano Lett.*, 2008, **8**(10), 3498–3502, DOI: 10.1021/nl802558y.

190 D. Moitra, C. Anand, B. K. Ghosh, M. Chandel and N. N. Ghosh, One-Dimensional $BiFeO_3$ Nanowire-Reduced Graphene Oxide Nanocomposite as Excellent Supercapacitor Electrode Material, *ACS Appl. Energy Mater.*, 2018, **1**(2), 464–474, DOI: 10.1021/acsaem.7b00097.

191 K.-P. Cheng, R.-J. Gu and L.-X. Wen, Application of a Clustered Countercurrent-Flow Micro-Channel Reactor in the Preparation of $KMnF_3$ Perovskite for Asymmetric Supercapacitors, *RSC Adv.*, 2020, **10**(20), 11681–11693, DOI: 10.1039/D0RA01411G.

192 P. M. Shafi, V. Ganesh and A. C. Bose, $LaMnO_3$/RGO/PANI Ternary Nanocomposites for Supercapacitor Electrode Application and Their Outstanding Performance in All-Solid-State Asymmetrical Device Design, *ACS Appl. Energy Mater.*, 2018, **1**(6), 2802–2812, DOI: 10.1021/acsaem.8b00459.

193 M. Riaz, T. Munawar, F. Mukhtar, M. S. Nadeem, S. Manzoor, M. N. Ashiq and F. Iqbal, Facile Synthesis of Polyaniline-Supported Halide Perovskite Nanocomposite (KCuCl3/PANI) as Potential Electrode Material for Supercapacitor, *J. Mater. Sci.: Mater. Electron.*, 2022, **33**(32), 24462–24476, DOI: 10.1007/s10854-022-09159-9.

194 A. Bibi, A. Shakoor, M. Raffi, M. Hina, N. A. Niaz, S. A. Fatima and M. N. Qureshi, Exploring the Potential of Polyaniline-Calcium Titanate (PANI-CaTiO3) Nanocomposites in Supercapacitors: Synthesis and Electrochemical Investigation, *J. Energy Storage*, 2024, **78**, 110321, DOI: 10.1016/j.est.2023.110321.

195 J. Huang, K. Jiang, D. Tranca, C. Ke, L. Zhang, J. Li, J. Li, G. Tong, E. Kymakis and X. Zhuang, Perovskite Oxide and Polyazulene–Based Heterostructure for High–Performance Supercapacitors, *J. Appl. Polym. Sci.*, 2021, **138**(41), 51198, DOI: 10.1002/app.51198.